Structural modeling of transition-metal–metalloid glasses by use of tight-binding-bond forces

Ch. Hausleitner and J. Hafner
Institut für Theoretische Physik, Technische Universität Wien, Wiedner Hauptstrasse 8-10, A-1040 Wien, Austria
(Received 22 June 1992)

A recently developed tight-binding-bond approach for the calculation of interatomic forces in disordered materials is extended to amorphous transition-metal–metalloid alloys. It is shown that the interaction of the transition-metal *d* electrons with the metalloid *p* electrons leads to strong covalent bonding forces that are reflected in a pronounced nonadditivity of the pair interactions. The structure of the amorphous alloys is modeled by a simulated molecular-dynamics quench. Results for Fe-B, Ni-B, Fe-P, and Ni-P glasses are in good agreement with diffraction experiments. It is shown that the covalent bonding forces lead to a chemical and topological order similar to that postulated in stereochemically defined models based on the packing of trigonal prismatic units. The molecular-dynamics simulations also predict a medium-range order (concentration fluctuations on a scale of 15–20 Å) in agreement with the existing small-angle scattering data.

I. INTRODUCTION

Metallic glasses may be synthesized from many different combinations of materials: (i) alloys of simple metals, (ii) alloys of transition metals, (iii) combining a transition metal or noble metal with a simple metal, (iv) combining a transition metal with a lanthanide or actinide element, and (v) combining a transition-metal with a metalloid. Historically, the glass-forming ability was first discovered in metal-metalloid systems.[1,2] Even today, the metal-metalloid glasses [especially (Fe,Co,Ni)-(B,P) glasses] are the most important candidates for large-scale technical applications.[3,17]

Because of the central importance of the metal-metalloid glasses, much effort has been spent to explore their structural, electronic, and magnetic properties. Experimentally, the atomic structure is well characterized at the level of partial correlation functions by detailed diffraction studies.[4–9] X-ray-absorption investigations [extended x-ray-absorption fine structure (EXAFS) and x-ray absorption near-edge structure (XANES)] provide at least some information on higher-order correlation functions.[10] All results point to a strong chemical and topological short-range order (SRO). The electronic structure has been investigated using photoemission spectroscopy,[11–13] electron-energy-loss spectroscopy,[14] and soft x-ray emission spectroscopy.[15,16] The electronic structure is found to be characterized by a relatively narrow transition-metal (TM) *d* band close to the Fermi level and a strong bonding-antibonding splitting in the metalloid (M) *p* band, indicating a strong covalent TM-M interaction. The magnetic properties of the metal-metalloid glasses have been measured[17–19] and the relation between atomic and magnetic structure has been discussed.[20] For higher metalloid concentrations (more than 10%), the magnetic moment per Fe atom decreases roughly linear with increasing metalloid content. The extrapolated values for pure Fe and Co seem to agree with the magnetic moments of the pure crystalline elements. However, results on Fe-rich samples[18] (more than 90% Fe) indicate a rather low magnetic moment.

Although the field seems to be experimentally well covered, progress in the theoretical treatment has been rather slow. The atomic structure seems to be rather well understood in terms of stereochemically defined models[21] based on the random packing of trigonal prismatic units that are thought to be characteristic for the crystalline borides, phosphides and silides.[22] Atomistic modeling studies have been performed using parametrized pair interactions.[5,23–28] After suitable adjustment of the interatomic forces, some of thee models are quite successful. However, they cannot establish a connection between the strong local chemical and topological order characteristic for these materials and the electronic structure.

The electronic structure of the TM-M glasses has been discussed on the basis of self-consistent local-density-functional calculations for simple crystalline reference structures,[29] and using non-self-consistent tight-binding calculations for amorphous models.[30] Self-consistency for an average atom in the glassy model has been achieved in the tight-binding linear-muffin-tin orbital (LMTO) calculations of Fujiwara,[16,31] local self-consistency in the tight-binding calculations of Ching *et al.*[32–34] In a spin-polarized version, the tight-binding approach has also been extended to a calculation of the magnetic moments.[35] No attempt has been made to derive interatomic forces from the electronic structure. This would be the missing cornerstone in a microscopic theory of the structure-property relationship for transition-metal–metalloid glasses.

The calculation of interatomic forces for materials with a strong covalent character of the chemical bond is a difficult task. Very recently, some progress has been achieved through the revival of an old concept: the bond order.[36,37] It has been shown that within tight-binding Hückel theory the quantum-mechanical bond energy in a given pair of atoms *i* and *j* can be written in the form[38–40]

$$U_{\text{bond}}(ij)=2t(R_{ij})\Theta_{i,j} , \quad (1)$$

i.e., as the product of the bond integral $t(R_{ij})$ between atoms located at a distance R_{ij} and the bond order Θ_{ij}. The bond order is defined as the difference in the number of electrons in bonding and antibonding states formed by the local orbitals on sites i and j. Equation (1) represents only formally a pair interaction, the quantum-mechanical many-body character of the interatomic forces enters through the bond order. For disordered intertransition-metal alloys we have shown that the bond order for the covalent interaction in the d band may be calculated analytically on a Bethe lattice reference system.[41] In the Bethe lattice approximation, the bonding interaction (1) reduces to a pair interaction in the spirit of an embedded-atom (or rather embedded-bond) approach: the pair forces depend on atomic environment through the coordination number and the bond length. We have shown that the electronic density of states calculated in the Bethe lattice approximation is a reasonably realistic approximation to the electronic spectrum of transition-metal glasses,[42] in particular it reproduces the d-band shift to higher binding energies with increasing difference in the components valence observed in the photoelectron spectra.[43] In the tight-binding-bond forces, the change in the electronic spectrum is reflected in an increasing nonadditivity of the interatomic forces arising from the covalent d-d interactions. Combined with a conventional pseudopotential description of the s-electron contribution to the chemical bonding forces, this hybridized nearly free-electron tight-binding-bond approach allows an atomistic modeling of the transition-metal glasses that explains all significant details of the amorphous structure.[44,45]

In the present paper we present an extension of the tight-binding-bond approach to transition-metal–metalloid systems. Our approach is inspired by the results of recent investigations of the bonding in transition-metal borides and phosphides.[46–49] In the TM-TM glasses, the bonding properties are determined by the tightly bound d-band complex of both metals and a common nearly free-electron-like s band [see Fig. 1(a)]. For the TM-M glasses the following model for the valence-band structure is appropriate in the metal-rich regime: the TM-d band close to the Fermi level interacts strongly with the M-p band. The TM-s states form a broad free-electron band, while the M-s states form a low-lying noninteracting band [Fig. 1(b)]. The last assumption could be problematic in the crystalline mono- and semiborides where a direct B-B interaction leads to appreciable s-p hybridization. According to all evidence, no direct B-B neighbors exist in the TM-rich metallic glasses, so that for our purposes this assumption seems to be well justified.

We follow again the strategy to compute the TM-s contribution to the interatomic forces in a nearly free-electron approximation (pseudopotentials and linear screening), and to calculate the forces from the TM-d and M-s,p electrons using the tight-binding-bond approach on a Bethe lattice.[50] Here we have to remember that the Bethe lattice defines an effective medium surrounding a

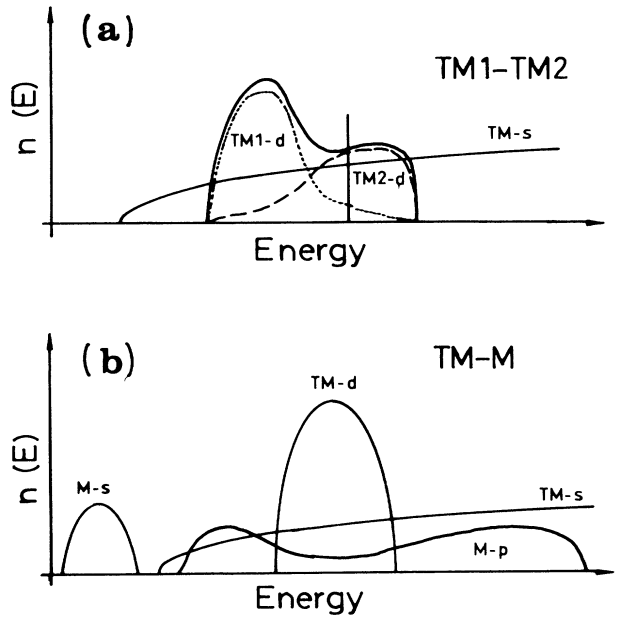

FIG. 1. Models for the valence-band structure of (a) intertransition-metal and (b) transition-metal–metalloid alloys.

given bond. In the Bethe lattice approach, this effective medium is characterized solely by the coordination numbers and the interatomic distances. For the close-packed TM-TM glasses we found it a good approximation[41,44] to assume an average coordination number of $Z=12$ and to neglect the small variations of the interatomic forces with local fluctuations in the coordination. In the TM-M glasses, the situation is different. There is ample evidence that in the crystalline T_3M compounds, as well as in the T_xM_{1-x} glasses with $x\approx 0.85-0.75$ the average coordination numbers are $Z_{\text{TM}}\sim 12$ on the metal sites and $Z_{\text{M}}\sim 9$ on the metalloid sites.[21] Therefore, we have to use a Bethe lattice reference system on which the coordination number is different for both species. Two-component Bethe lattices with two different coordination numbers have already been used as models for the electronic[51] and magnetic[52] properties of amorphous alloys. Details of the theory are worked out in Sec II. We find that the strong covalent interactions lead to strong attractive TM-M and TM-TM nearest-neighbor interactions, whereas the M-M interactions are attractive only for distances corresponding to second neighbors.

Section III presents detailed molecular-dynamics modeling studies based on these quantum-mechanical pair forces. We show that although the agreement with experiment is not as perfect as for the TM-TM glasses, the results are nonetheless very encouraging, especially for the phosphide glasses. For the borides, like for any compounds of first-row elements, the tight-binding parametrization of the valence band is notoriously difficult. Still, the simulated structures are sufficiently realistic to allow the differences in the structures of the B- and P-based glasses to be traced back to the differences in the valence band structure. Our conclusions are presented in Sec. IV.

II. INTERATOMIC FORCES IN TRANSITION-METAL–METALLOID GLASSES

A. The hybridized nearly free-electron tight-binding-bond (NFE-TBB) concept

For a transition-metal system with nearly free s and tightly bound d electrons we assume that the total energy may be decomposed into contributions from s and d electrons.[41]

$$E_{\rm tot}=E_s+E_{\rm TB} \ . \tag{2}$$

The s-electron part is treated in standard pseudopotential perturbation theory,[53,54] expressing E_s in terms of a volume energy $E_0(\Omega)$ and a sum over density-dependent pair potentials $\Phi_s(R;\Omega)$. For the tight-binding contribution it has been shown[38] that the variational property of the ground-state energy in the local-density approximation allows one to decompose $E_{\rm TB}$ into a repulsive pair-interaction term accounting for the electrostatic, exchange-correlation, and nonorthogonality terms, and a covalent bond energy $E_{\rm bond}$,

$$E_{\rm TB}=\frac{1}{2N}{\sum_{i,j}}'\Phi_{\rm rep}(R_{ij})+E_{\rm bond} \ . \tag{3}$$

The bond energy represents the gain in energy arising from the formation of a band with the local density of states $n_i(E)$. Within a one-band approximation, one has (E_F is the Fermi energy)

$$\begin{aligned}E_{\rm bond}&=\sum_i\int^{E_F}(E-E_i)n_i(E)dE\\&=E_{\rm band}-\sum_i N_iE_i \ .\end{aligned} \tag{4}$$

The last equality relates the bond energy to the band energy, i.e., to the sum of the one-electron energy eigenvalues. E_i is the on-site energy, and N_i stands for the number of d electrons on site i.

The one-band approximation assumes that the TB-d orbitals are degenerate and neglects the directionality of the d-d bonds. This is, of course, of questionable validity for crystalline systems, but appears to be a legitimate first approximation in a disordered (liquid or glassy) system. It follows that in a two-center orthogonal TB approach, the bond energy is given by[39,55]

$$E_{\rm bond}=\frac{1}{2N}{\sum_{i,j}}'t_{ij}(R_{ij})\Theta_{ij} \ , \tag{5}$$

where t_{ij} is the transfer integral and Θ_{ij} the bond order. The bond order is defined as the difference of the number of electrons in the bonding and antibonding states formed by the TB orbitals on sites i and j. It can be expressed in terms of the off-diagonal Greens function via

$$\Theta_{ij}=-\frac{2}{\pi}\int^{E_F}{\rm Im}G_{ij}(E)dE \ . \tag{6}$$

Formally, Eq. (4) defines a pair interaction, but the many-body character of the covalent bond enters via the bond order—in general, Θ_{ij} depends on the local environment of the (ij) bond.

B. Application of the NFE-TBB concept to TM-M glasses

Our extension of the NFE-TBB concept to TM-M glasses is based on the following assumptions: (i) the TM-s electrons form a NFE band, (ii) the M-s atoms form a full, nonbonding band separated from the lower part of the valence band, (iii) the TM-d and M-p bands form a strongly hybridized TB-band complex, (iv) a one-band approximation is appropriate for both TM-d and M-p states. This means that the chemical occupation of a given site specifies at the same time the angular momentum quantum number of the TB orbital. In the following we shall use a single Greek index α to label at the atomic species and the quantum number, i.e., α=TM,d or α=M,p. The numbers N_s and N_d of TM-s and d electrons are taken to be equal to the results of self-consistent band-structure calculations for the crystalline TM metals,[56] for the metalloid atoms the number of p electrons is always equal to their number in the free atom.

A major problem in electronic structure and total-energy calculations in binaries consists in the charge transfer and the large and mutually compensating changes in the band energy and in the electrostatic and exchange-correlation contributions arising from the charge redistributions. The local-force theorem[57,58,59] of density-functional theory shows that to first order in the charge redistribution this compensation is exact, so that the change in energy is given to first order by the change of the band energy for a frozen potential. Moreover, within TB theory, Pettifor[55] has shown that the change of the band energy at fixed on-site energy (corresponding to a frozen potential) is equal to the change of the bond energy at fixed orbital occupancy. If the orbital occupancy in the alloy is equal to that in the pure metals, the contribution of the promotion energy to the alloy energy vanishes (see the detailed discussion in Ref. 41). With this constraint of local charge neutrality, the decomposition of the tight-binding energy into a repulsive pairwise term and a bond energy remains valid for a binary system.

However, as the local-force theorem is valid only to first order in the change in the charge density, one has to verify that the use of this theorem is justified under the given circumstances. One possibility is to compare the approximate density of states calculated on the reference systems (see below) used for the calculation of the bond order and the interatomic forces with the exact density of states (DOS) determined for the structure calculated by molecular dynamics using these pair forces. For the intertransition-metal glasses it has been shown that the approximate DOS calculated on the Bethe lattice reference system compares well with the exact DOS of the computer-generated models, calculated using a LMTO supercell method.[41] Similar tests for the TM-M glasses are now under preparation.

The bond order $\Theta_{ij}^{\alpha\beta}$ has to be calculated on an appropriately chosen reference system. For the TM-TM glasses we have shown that a Bethe lattice[50] is sufficiently realistic to reproduce the main features of the d-band complex (transition from common-band to split-band form with increasing difference in the d-band occupancy of the two metals). The Bethe lattice is characterized by the length of a nearest-neighbor bond and the coordinate

number Z. The bond order has an inverse square-root dependence on the coordination number (with a scaling assumption for the second moment of the electronic DOS, this results in the usual $\sqrt{Z}$ dependence of the tight-binding energy).[41] With the high average coordination number characteristic for TM-TM glasses ($\bar{Z}\sim 12$), the influence of small local fluctuations in the coordination on the interatomic potentials can be neglected. The situation is different in the TM-M glasses. There is sufficient evidence for significant differences in the TM- and M-coordination numbers.[21] The analysis of the diffraction and EXAFS data shows that in all T_xM_{1-x} glasses with $0.75<x<0.85$, we have $Z_{\mathrm{TM}}\sim 12$ and $Z_M\sim 9$ (see Ref. 21). The Bethe lattice approach to the electronic DOS can be generalized to the case where the coordination number depends on the site occupation.

On a binary Bethe lattice the degree of chemical order has to be specified. The partial coordination numbers are given by

$$Z_{\alpha\beta}=p_{\alpha\beta}Z_\alpha,\quad \alpha,\beta=A,B\ , \tag{7}$$

where $p_{\alpha\beta}$ is the probability that an α atom has a β neighbor and

$$Z_\alpha=Z_{\alpha\alpha}+Z_{\alpha\beta},\quad \alpha,\beta=A,B,\quad \alpha\neq\beta \tag{8}$$

is the total coordination number for the species α. For a random distribution of the two chemical species, we have $p_{\alpha\beta}=x_\beta$ where x_β is the concentration of β.

III. CALCULATION OF THE BOND ORDER ON A BETHE LATTICE

For a Bethe lattice with nearest-neighbor interactions only, renormalized perturbation theory leads to the following relations for the diagonal and off-diagonal Greens functions, G_{ii}^α and $G_{ij}^{\alpha\beta}$, and for the self-energy Δ_i^α,

$$G_{ii}^\alpha(E)=[E-E_i^\alpha-\Delta_i^\alpha]^{-1},\quad \alpha=A,B\ , \tag{9}$$

$$G_{ij}^{\alpha\beta}(E)=S_{\alpha\beta}G_{jj}^\beta(E),\quad \alpha,\beta=A,B\ , \tag{10}$$

$$\Delta_i^\alpha(E)=Z_{\alpha\alpha}t_{\alpha\alpha}S_{\alpha\alpha}+Z_{\alpha\beta}t_{\alpha\beta}S_{\beta\alpha}\ ,\quad \alpha,\beta=A,B,\quad \alpha\neq\beta\ , \tag{11}$$

where $t_{\alpha\beta}$ are the nearest-neighbor transfer (hopping) integrals. The transfer matrices $S_{\alpha\beta}$ are determined by the solution of the four simultaneous equations

$$(E-E_j^\beta)S_{\beta\alpha}=t_{\alpha\beta}+\sum_{\tau=1}^{Z_\beta-1}t_{\beta\gamma(\tau)}S_{\gamma(\tau)\beta}S_{\beta\alpha}\ ,\qquad \alpha,\beta,\gamma=A,B\ . \tag{12}$$

For details of the derivation, see Ref. 41. Equations (10)–(12) correspond to a situation where we have an α atom at site i and a β atom at a nearest-neighbor site j (coupled through $t_{\alpha\beta}$), the index τ labels the $(Z_\beta-1)$ neighbors of type $\gamma(\tau)$ of site j (with the exception of the α atom at site i). Taking a configuration average and solving for $S_{\beta\alpha}$ leads to

$$S_{\beta\alpha}=t_{\alpha\beta}\left[E-E_j^\beta-(Z_\beta-1)\sum_\gamma p_{\beta\gamma}t_{\beta\gamma}S_{\gamma\beta}\right]^{-1}\ ,\qquad \alpha,\beta,\gamma=A,B\ . \tag{13}$$

Considering that the off-diagonal elements of the transfer matrix obey the relations

$$S_{\alpha\beta}=\frac{t_{\alpha\beta}}{t_{\alpha\alpha}}S_{\alpha\alpha},\quad \alpha,\beta=A,B,\quad \alpha\neq\beta\ , \tag{14}$$

the four equations (13) reduce to two quadratic equations for the diagonal elements

$$S_{\alpha\alpha}=t_{\alpha\alpha}\left[E-E_j^\alpha-(Z_\alpha-1)\times\left[p_{\alpha\alpha}t_{\alpha\alpha}S_{\alpha\alpha}+p_{\alpha\beta}\frac{t_{\alpha\beta}^2}{t_{\beta\beta}}S_{\beta\beta}\right]\right]^{-1}\ ,\qquad \alpha,\beta=!,B,\quad \alpha\neq\beta\ . \tag{15}$$

Solving for $S_{\alpha\alpha}$ yields a quartic equation

$$A_4S_{\alpha\alpha}^4+A_3S_{\alpha\alpha}^3+A_2S_{\alpha\alpha}^2+A_1S_{\alpha\alpha}+A_0=0\ . \tag{16}$$

Explicit expressions for the coefficients A_i, $i=0,4$, are given in the Appendix. These relations are more complex than the corresponding relations for the TM-TM glasses given in Ref. 41 because the coordination number depends on the site occupation.

The quartic equation (15) has to be solved numerically. The physical solution is determined by the condition that the partial densities of states $n_\alpha(E)=(1/\pi)\,\mathrm{Im}G_{ii}^\alpha(E)$ calculated via (9) and (8) are positive semidefinite. Combining Eqs. (13) and (14) with Eqs. (8)–(10), we find that the off-diagonal Greens function for nearest-neighbor sites is given by

$$G_{ij}^{\alpha\beta}=S_{\alpha\beta}G_{jj}^\beta=\frac{t_{\alpha\beta}}{\{E-E_j^\alpha-[(Z_\alpha-1)/Z_\alpha]\Delta_j^\alpha\}(E-E_j^\beta-\Delta_j^\beta)}\qquad \alpha,\beta=A,B,\alpha\neq\beta\ . \tag{17}$$

Equation (17) shows that due to the factor $(Z_\alpha-1)/Z_\alpha$ in the denominator, $G_{ij}^{\alpha\beta}\neq G_{ij}^{\beta\alpha}$. However, the difference is small for large coordination numbers and vanishes in the limit $Z_\alpha,Z_\beta\to\infty$. The bond order in an α,β bond is approximated by the arithmetic mean of the two off-diagonal Greens functions, i.e.

$$\Theta_{ij}^{\alpha\beta}=-\frac{2}{\pi}\int^{E_F}\mathrm{Im}[\tfrac{1}{2}(S_{\alpha\beta}G_{jj}^\beta+S_{\beta\alpha}G_{jj}^\alpha)]dE\ ,\qquad \alpha,\beta=A,B\ . \tag{18}$$

A. TB parametrization of the electronic Hamiltonian and bonding pair interaction

The tight-binding parametrization of the electronic Hamiltonian for transition-metal–metalloid systems is a nontrivial task. B and P, the most important metalloids in metallic glasses, occur in various complex polymorphic structures characterized by low coordination numbers and low packing fractions. This is very different from the dense-packing characteristic for the metallic glasses, so

that the transferability of the TB parameters represents a certain problem (for the construction of transferable TB parameters for covalently bonded systems, see also Goodwin, Skinner, and Pettifor[60]). We approach this problem by deriving the TB parameters for the metalloid atoms from self-consistent band-structure calculations for hypothetical high-symmetry polymorphs.

In general, the average *p-p*, *p-d*, and *d-d* transfer integrals for our one-band per site model are given in a second-moment approximation[61] by

$$t_{pp}(R_{ij})=\sqrt{\tfrac{1}{3}[t_{pp\sigma}^2(R_{ij})+2t_{pp\pi}^2(R_{ij})]}\ , \tag{19}$$

$$t_{pd}(R_{ij})=\sqrt{\tfrac{1}{3}[t_{pd\sigma}^2(R_{ij})+2t_{pd\pi}^2(R_{ij})]}\ , \tag{20}$$

$$t_{dd}(R_{ij})=\sqrt{\tfrac{1}{5}[t_{dd\sigma}R_{ij})+2t_{dd\pi}^2(R_{ij})+2t_{dd\delta}^2(R_{ij})]}\ . \tag{21}$$

Note that with (20), $t_{pd}\neq\sqrt{t_{pp}t_{dd}}$. The approximation of t_{pd} by the geometric mean is common practice in TB calculations and referred to as Shiba's approximation.[62]

The σ, π, and δ transfer integrals may be expressed in terms of the tight-binding radii R_l, $l=p,d$ of Harrison[61,63] via

$$t_{l_\alpha l_\beta m}(R)=\eta_{l_\alpha l_\beta m}\frac{\hbar^2}{m}\frac{\sqrt{R_{l_\alpha}^{2l^\alpha-1}R_{l_\beta}^{2l_\beta-1}}}{R^{l_\alpha+l_\beta+1}}\ ,$$
$$l_a,l_\beta=p,d,\ m=\sigma,\pi,\delta \tag{22}$$

(see the Solid State Tables of Harrison[63] for the values of the coefficients $\eta_{l_\alpha l_\beta m}$).

For the transition metals $R_l=R_d$ can be fitted to the canonical *d*-band width of Andersen and Jepsen.[64] To obtain $R_l=R_p$ for the metalloids, we use the expression for the *p*-band width in the atomic surface method of Harrison and Straub[65] [valid for body-centered-cubic (bcc) and simple-cubic (sc) lattices]:

$$W_p=\frac{8}{\pi}\frac{\hbar}{m}\frac{R_p}{d_{\rm bcc}^3}\ , \tag{23}$$

where $d_{\rm bcc}$ is the nearest-neighbor distance in the bcc lattice. The bandwidth W_p may be taken from self-consistent band-structure calculations[56] for the hypothetical bcc phase at the theoretical equilibrium density. However, the equilibrium volume of the bcc phase is much smaller than that of the observed low-symmetry phases of B and P. It has been shown that for the TB analysis of the stability of the open covalent structures, the second-moment scaling assumption has been quite successful.[66,67] An invariant second moment of the electronic DOS is equivalent to a scaling of the TB radius according to

$$R_{p,\rm sc}=R_{p,\rm bcc}\left[\frac{d_{\rm sc}}{d_{\rm bcc}}\right]^3 \tag{24}$$

for a change from a bcc to a sc lattice. The metalloid TB radius to be used in the TM-M glasses is taken to be equal to that of a sc metalloid lattice with the atomic volume of the stable crystalline phase. The choice of a sc reference structure is motivated by the fact that the bond length $d_{\rm sc}$ is about equal to the shortest B-B (or P-P) distance in the glasses. Admittedly, this procedure bears some arbitrariness. It is justified by the fact that the Bethe lattice DOS calculated with these parameters gives a tolerably realistic account of the electronic band structure of the Fe and Ni borides and phosphides (cf. below) and ultimately by the success of the resulting interatomic forces.

For the $(ss\sigma)$ interactions between the metalloid atoms, Eq. (20) leads to an unrealistic R^{-1} dependence of the transfer integrals. For the *s,p*-bonded compounds of the main-group elements, Harrison[63] proposed to treat *s* and *p* electrons on a common basis, with transfer integrals varying as R^{-2}, as suggested by the lattice-parameter dependence of the free-electron bands. This can hardly be expected to be a good approximation for the narrow *s* bands of the phosphides and borides. If we neglect *s-p* hybridization, there will be no contribution of the *s* electrons to the bonding pair interaction, since the bond order of a completely filled nonhybridized band is always zero. However, the *s* electrons contribute to the repulsive potential as discussed below.

The on-site energies E_i^α are calculated for the transition metals for the s^1d^{N-1} (N is the group number) of the free atoms, for the metalloids they are taken from the Solid State Tables of Harrison.[63] This completely specifies the input for the calculation of the attractive bonding forces. The bond order $\Theta_{ij}^{\alpha\beta}$ follows from Eqs. (16)–(18). Together with (4) this defines a bonding pair interaction

$$\Phi_{\alpha\beta,\rm bond}(R_{ij})=t_{\alpha\beta}(R_{ij})\Theta_{ij}^{\alpha\beta}\ . \tag{25}$$

In (25) we have assumed that the distance dependence of the bond order is negligible against that of the transfer integral.

B. Repulsive TB pair interaction

For the parametrization of the repulsive pair interactions we follow Wills and Harrison.[61] The dominant contribution comes from the overlap integrals, $\Phi_{\alpha\beta,\rm rep}$ is given by

$$\Phi_{\alpha\beta,\rm rep}(R_{ij})=-\frac{2\sqrt{N_i^\alpha N_j^\beta}}{2l_\alpha+1}\sum_m O_{l_\alpha l_\beta m}(R_{ij})t_{l_\alpha l_\beta m}(R_{ij})\ , \tag{26}$$

$$l_\alpha\le l_\beta\ ,\quad m=\sigma,\pi,\delta\ . \tag{27}$$

N_i^α stands for the number of electrons in TB states (in our model either $N_{\rm M}^p$ for the metalloid and $N_{\rm TM}^d$ for the transition-metal sites). The overlap integrals are given in terms of the TB radii by

$$O_{l_\alpha l_\beta m}(R_{ij})=\sigma_{l_\alpha l_\beta m}\frac{\sqrt{R_{l_\alpha}^{2l_\alpha-1}R_{l_\beta}^{2l_\beta-1}}}{R_{ij}^{l_\alpha+l_\beta-1}}\ ,l_\alpha,l_\beta\neq 0 \tag{28}$$

with

$$\sigma_{l_\alpha l_\beta m} = -\frac{1}{2(l_\alpha + l_\beta)}\left[1+\frac{4m^2-1}{(2l_\alpha-1)(2l_\beta-1)}\right]\eta_{l_\alpha l_\beta m} \ . \tag{29}$$

Equations (26)–(29) and (22) lead to an R^{-8}, R^{-6}, and R^{-4} distance dependence of the repulsive (d-d), (d-p), and (p-p) interactions, Eqs. (22) and (25) to an R^{-5}, R^{-4}, and R^{-3} distance dependence of the bonding (d-d), (p-d), and (p-p) pair interactions.

C. TM-*s* and M-*s* electron contributions to the pair interactions

The contribution of the TM-s electrons to the pair potentials is calculated using pseudopotential perturbation theory. As in our work on the TM-TM glasses,[41] we use an empty-core form[54,68] for the TM-pseudopotential, with the empty-core radius R_c fitted to the structure of the pure liquid transition metals.[69] For the dielectric screening function we use the Ichimaru-Utsumi[70] local-field corrections to the Hartree dielectric function.

Although the M-s electrons do not contribute to the bonding forces, their contribution to the repulsive interactions is non-negligible—at least for the borides. However, the canonical parametrization (26) and (27) of $\Phi_{\rm rep}$ is unphysical for s states, and the Harrison parametrization assuming $\Phi_{\rm rep} \propto R^{-4}$ was shown to yield inaccurate results for first-row elements such as C and B (Ref. 60). For C it was shown that the hopping integrals and the pair potentials fitted to the band structures, binding energies, and lattice constants of the graphite and diamond structures decay more rapidly than for silicon, reflecting the absence of nuclear screening by the core-electron states. The fitting procedure leads to exponents

TABLE I. Top: Input data for the calculation of the interatomic forces. Middle: Number densities for the amorphous alloys. Bottom: Bond order $\Theta_{ij}^{\alpha\beta}$ for covalent interactions in TM-M alloys calculated on a random Bethe lattice with different partial coordination numbers Z_α.

	$\Omega_{\rm at}$ (Å^3)	N_s	$N_{d(p)}$	E^α (eV)	R_l (Å)	R_c (Å)
Fe	11.78	1.42	6.58	−5.58	0.840	0.80
Ni	10.04	1.40	8.60	−6.49	0.744	0.58
B	7.79		1	−7.55	10.76	
P	18.99		1	−11.05	16.34	

	n (Å^{-3})		n (Å^{-3})
$Ni_{81}B_{19}$	0.0967	$Fe_{80}B_{20}$	0.0950
$Ni_{64}B_{36}$	0.1020	$Fe_{80}P_{20}$	0.0840
$Ni_{80}P_{20}$	0.0890	$Fe_{76}P_{24}$	0.0830

T_xM_{1-x}	$\Theta^{dd}_{\rm TM\text{-}TM}$	$\Theta^{dp}_{\rm TM\text{-}M}$	$\Theta^{pp}_{\rm M\text{-}M}$
$Fe_{80}B_{20}$	−2.144	−1.349	−1.117
$Ni_{81}B_{19}$	−0.976	−1.411	−1.290
$Ni_{64}B_{36}$	−0.689	−1.321	−1.144
$Fe_{80}P_{20}$	−2.005	−1.670	−2.301
$Fe_{76}P_{24}$	−1.967	−1.640	−2.259
$Ni_{80}P_{20}$	−0.826	−1.499	−2.678

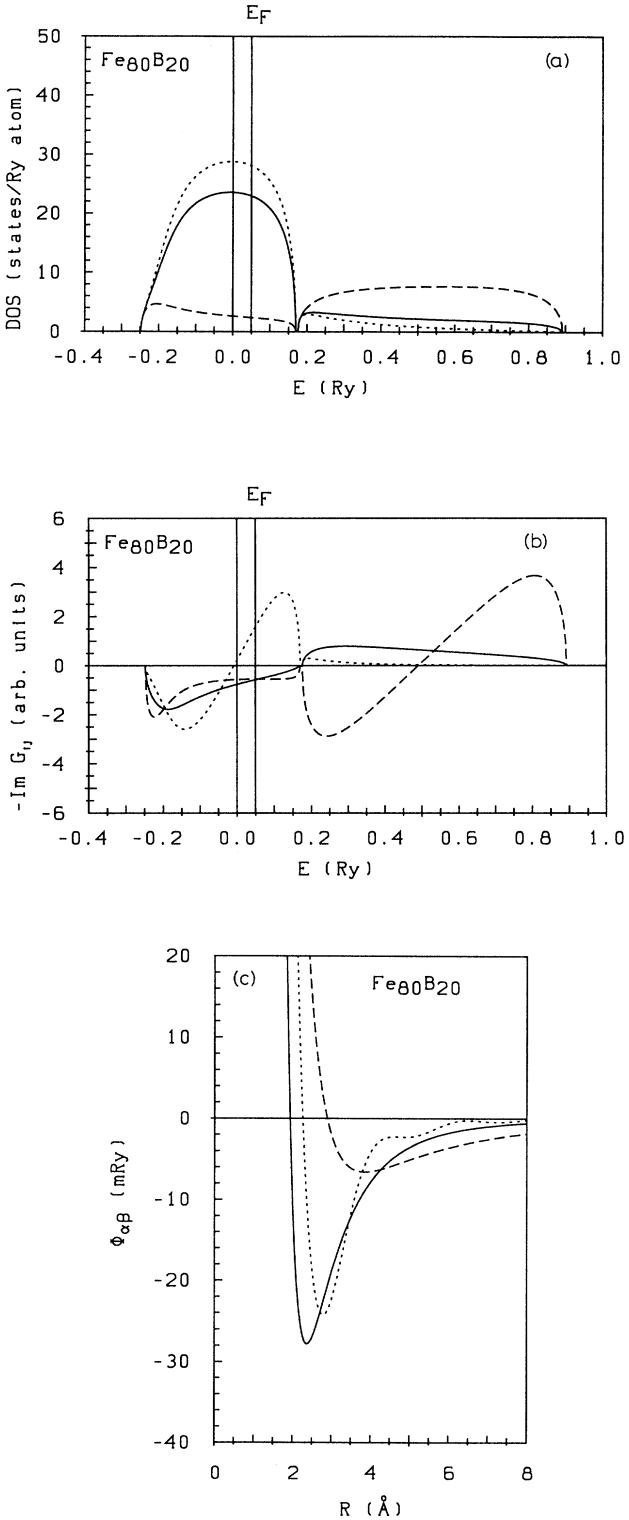

FIG. 2. (a) Total and partial electronic densities of state for $Fe_{80}B_{20}$, calculated on the Bethe lattice. Solid line, total; dotted line, TM; dashed line, M-DOS. The Fermi energy is marked by a vertical line. (b) Imaginary part of the off-diagonal Greens function for $Fe_{80}B_{20}$. Solid line, TM-M; dotted line, TM-TM; dashed line, M-M; TM=Fe, M=B. (c) Pair interactions for $Fe_{80}B_{20}$. Same symbols.

$n=-2.8$ for the hopping integral and $n=-4.5$ for the repulsive R^n pair potential.[60] The last value is very close to the R^{-4} law of the p-p pair potential resulting from the canonical parametrization. Therefore, to account for the s-electron repulsion we decided to proceed as follows: we multiply the $(pp\sigma)$ contribution to Φ_{rep} with an adjustable prefactor $f_{B(P)}$. $f_B=1$ corresponds to a neglect of the s-electron contribution. For the boride glasses we found that a value of $f_B\sim 2$ is necessary to avoid a clustering of B atoms and a tendency to phase separation (for details see below). For the phosphide glasses, the core screening and the less extended P-s states minimize the importance of the s-electron repulsion and accurate results are obtained with $f_B=1$. All input parameters for the calculation of the NFE-TBB pair and volume forces are compiled in Table I.

D. NFE-TBB potentials in TM-M glasses and their relation to the electronic structure

In the following we describe the application of the NFE-TBB concept to Fe-B, Fe-P, Ni-B, and Ni-P glasses. We discuss the results for the borides first. Figure 2 shows the total and partial DOS's for the p-d-band complex of $Fe_{80}B_{20}$. We find a relatively narrow Fe-d band and a very broad B-p band, the lowest part of the B-p band overlaps with the Fe-d band. The strong $(p$-$d)$ interaction leads to the formation of a narrow, hybridization-induced pseudogap about 0.1 Ry above the Fermi level. The DOS is in reasonable agreement with the self-consistent linear combination of atomic orbitals (LCAO) calculations of Ching *et al.*[48] for crystalline Fe_3B, with the TB-LMTO recursion calculations of Fujiwara[31] for empirical models of amorphous Fe_xB_{1-x} and with the non-self-consistent LCAO calculations of Ching and Xu[71] for amorphous $Fe_{80}B_{20}$. The imaginary part of the off-diagonal Greens functions is shown in Fig. 2(b). A negative value of $(-\mathrm{Im}G_{ij})$ represents a predominance of bonding states. We see that integration up to the Fermi level counts only bonding contributions for Fe-B and B-B interactions, whereas for Fe-Fe the bonding contributions are partially compensated by antibonding states. However, since only a few B-B bonding states are actually occupied, the B-B bond order is relatively weak (Table I). In the interatomic forces [Fig. 2(c)] this is reflected in a strong nonadditivity of the pair forces: the Fe-B potential has the smallest repulsive diameter (this leads to a very short Fe-B bond distance), and the strongest attractive forces. The partially filled d band leads to strong Fe-Fe interactions, the extended p states (see the TB radii in Table I) to a large repulsive diameter for the B-B interactions.

If Fe is substituted by Ni, the main effects are the slightly smaller difference in the on-site energies and, most important, the higher degree of filling of the TM-d band. The result of the change in the on-site energies is larger B-B and Ni-B bond orders (and more attractive pair interactions), the compensation of bonding and antibonding contributions leads to a low bond order and a weak pair potential for Ni-Ni pairs (Fig. 3).

The phosphides differ from the borides by the less extended p orbitals and smaller differences in the on-site energies. Consequently, the width of the M-p band is reduced and the M-p band has a larger overlap with the TM-d band with a large bonding-antibonding splitting for TM-M and M-M interactions (Figs. 4 and 5). Again, this is in good agreement with electronic-structure calculations on the crystalline and amorphous phosphides. Another important difference is in the larger repulsive diameter of the P-P interactions. In $Fe_{80}P_{20}$, the strength of all three pair interactions is about the same, but the Fe-P bond distance is predicted to be much shorter than the average of the Fe-Fe and P-P bond distance (Fig. 4). In $Ni_{80}P_{20}$ the narrower and nearly completely filled Ni-d band leads to very weak Ni-Ni forces and allows at the same time very strong covalent P-P interactions [see the

TABLE II. Partial coordination numbers and interatomic distances in T_xM_{1-x} glasses.

Alloy		Partial coordination numbers				Distances (Å)		
		$N_{TM\text{-}TM}$	$N_{TM\text{-}M}$	$N_{M\text{-}TM}$	$N_{M\text{-}M}$	$d_{TM\text{-}TM}$	$d_{TM\text{-}M}$	$d^{a}_{M\text{-}M}$
$Ni_{81}B_{19}$	Theor.	10.8	2.3	10.0	0.05	2.44	2.11	3.50,4.15
	Expt.	10.8	2.2	9.3		2.52	2.11	3.29,4.02
$Fe_{80}B_{20}$	Theor.	11.2	2.4	9.6	0.08	2.51	2.27	3.55,4.14
	Expt.[c]	12.4	2.2	8.6		2.57	2.14	3.57
$Ni_{80}P_{20}$	Theor.	9.9	2.8	11.3	0.6	2.46	2.39	4.08
	Exp.[d]	9.4	2.3	9.3		2.56	2.28	3.73,4.30
$Fe_{80}P_{20}$	Theor.	9.9	2.8	11.0	0.13	2.49	2.44	4.01,4.59
	Expt.[e]							
$Fe_{76}P_{24}$	Theor.	10.2	3.4	10.9	0.4	2.51	2.44	3.80,4.59
	Expt.[e]					2.62	2.46	3.61,4.55
$Ni_{64}B_{36}$	Theor.	9.9	5.0	8.8	1.2	2.46	2.21	2.53
	Expt.[f]	10.1	3.9	6.9	1.1	2.55	2.12	

[a]The shortest metalloid-metalloid distance are not nearest-neighbor distances.
[b]Reference 7.
[c]Reference 4.
[d]Reference 6.
[e]Reference 5.
[f]Reference 8.

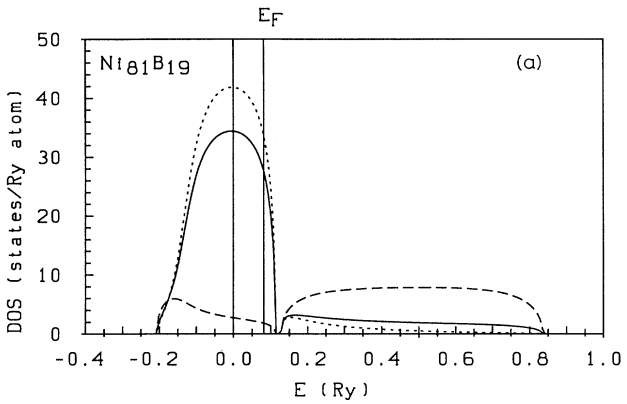

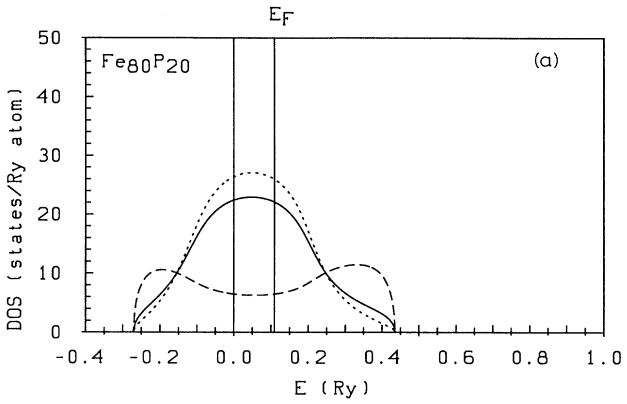

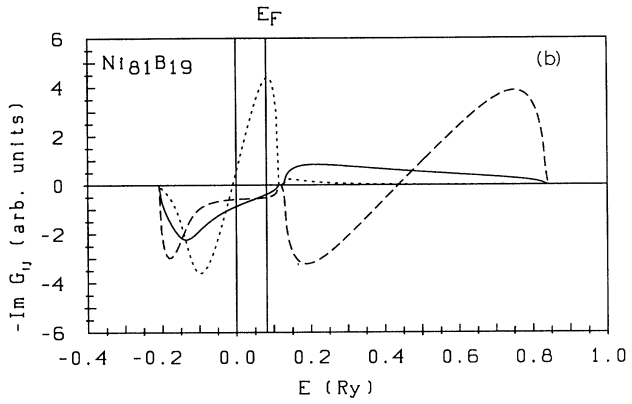

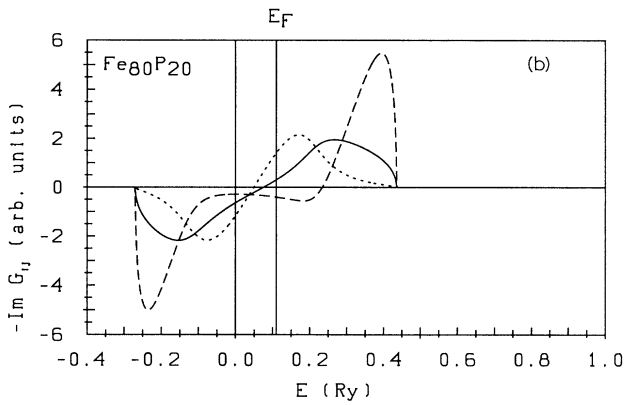

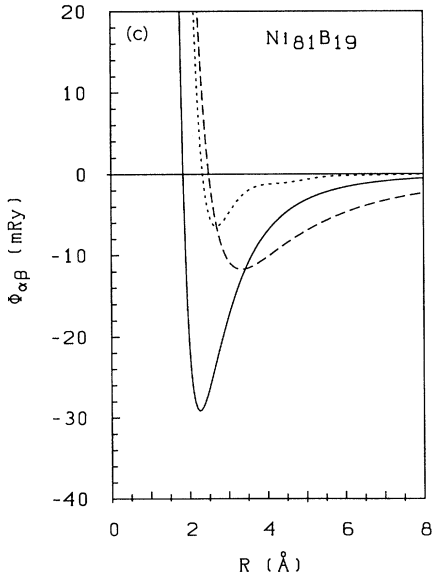

FIG. 3. (a)–(c) Total and partial electronic densities of state, off-diagonal Greens functions, and pair interactions for $Ni_{81}B_{19}$, calculated in the Bethe lattice approximation. For the key see Fig. 2.

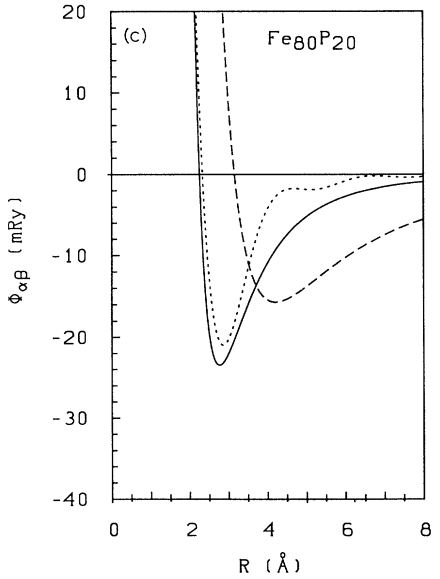

FIG. 4. (a)–(c) Total and partial electronic densities of state, off-diagonal Greens functions, and pair interactions for $Fe_{80}P_{20}$ calculated in the Bethe lattice approximation. For the key see Fig. 2.

off-diagonal Greens function for P-P bonds in Fig. 5(b)].

In alloys with a higher metalloid content, e.g., $Ni_{64}B_{36}$, there are only small changes in the Bethe lattice DOS, in the bond orders (see Table I) and in the pair interactions. However, the assumption of a nonbonding B-s band might become problematic with increasing B content.

IV. STRUCTURES OF TRANSITION-METAL METALLOID GLASSES

A. Molecular-dynamics modeling

We have performed microcanonical molecular-dynamics simulations of the liquid and glassy phases. For the integration of the Newtonian equations of motion we use a fourth-order predictor-corrector algorithm in the Nordsieck formulation,[72] with one iteration per corrector step. A net-cube approximation to the cutoff sphere is used for finding the atoms within the interaction radius around a given atom.[73,74]

Our simulations have been performed for $N=1372$ atoms in the molecular-dynamics cell, with a time increment $\Delta t=10^{-15}$ s. With this value of Δt, the total energy remains constant to within the four leading digits over several thousand integration steps. The interatomic potential is cut at a distance of about 25% of the cube edge of the molecular-dynamics cell. With this cutoff, each interaction sphere contains about 100 atoms.

The simulation was started in the liquid phase and a density corresponding to that of the glass and a temperature about 500 K above the liquidus of the equilibrium phase diagram. Typical runs took 4000–5000 steps for melting and equilibration and about as many for production. For a production of the glassy phase the system is quenched by lowering the temperature quasicontinously in 8000 time steps to $T=273$ K by scaling the velocities in intervals of 20 time steps. This corresponds to a quench rate of about $T\simeq 10^{14}$ K s^{-1}. After quenching the system is equilibrated for 2000 time steps, and finally 4000 times steps are used for calculating pair-correlation functions. Pair-correlation functions are based on averages of over 40 independent configurations taken at intervals of 100 times steps. Bond-angle distributions are calculated for only a small number of instantaneous configurations taken at larger time intervals. For further details of the simulation, we refer to Ref. 41.

B. Boron glasses

1. $Fe_{80}B_{20}$

Figure 6 shows the partial reduced correlation functions $G_{ij}(R)$ and the Faber-Ziman and Bhatia-Thornton structure factors for amorphous $Fe_{80}B_{20}$, compared with the neutron-diffraction data of Nold *et al.*[4] The partial structure factors of the computer-generated model are in good agreement with experiment. The Bhatia-Thornton structure factors show the strong chemical order in this glass, and a rather weak coupling between concentration and density fluctuations [$S_{NC}(Q)$ is very weak]. The par-

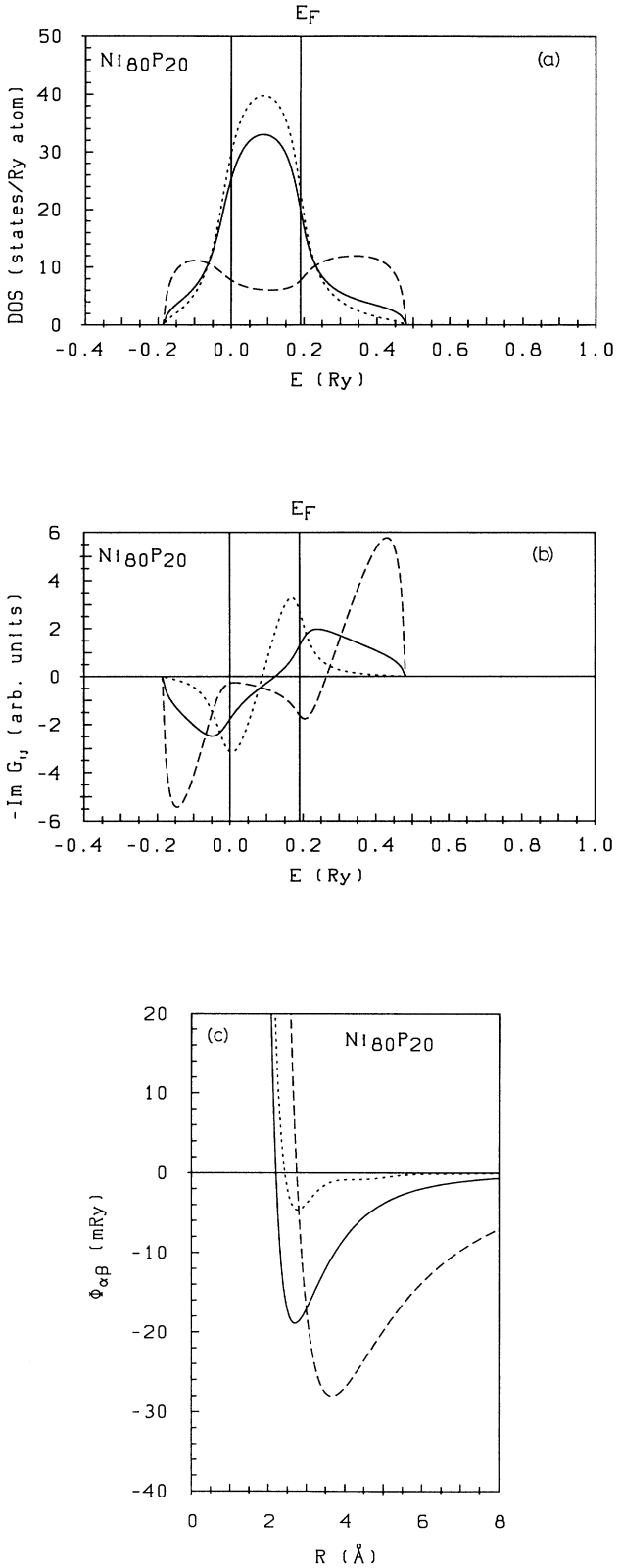

FIG. 5. (a)–(c) Total and partial electronic densities of state, off-diagonal Greens functions, and pair interactions for $Ni_{80}P_{20}$, calculated in the Bethe lattice approximation. For the key see Fig. 2.

tial correlation functions show that the only relevant discrepancies between theory and experiment are the overestimation of the nearest-neighbor Fe-B distance by 0.13 Å [otherwise interatomic distances are predicted with good accuracy (see Table II)], and a certain lack of structure in the second peaks of the Fe-Fe and Fe-B correlations. The B-Fe coordination number $N_{\text{B-Fe}} \sim 9$ is compatible with a local arrangement in the form of caped trigonal prisms. The total and partial bond-angle distribution functions (Fig. 7) also show that the local geometry around Fe and B sites is characteristically different. The distribution of the angles around the Fe sites has a main peak at 60° and flat maxima at 110°, 150°, and 180° [note that in Fig. 7 the frequency of the bond

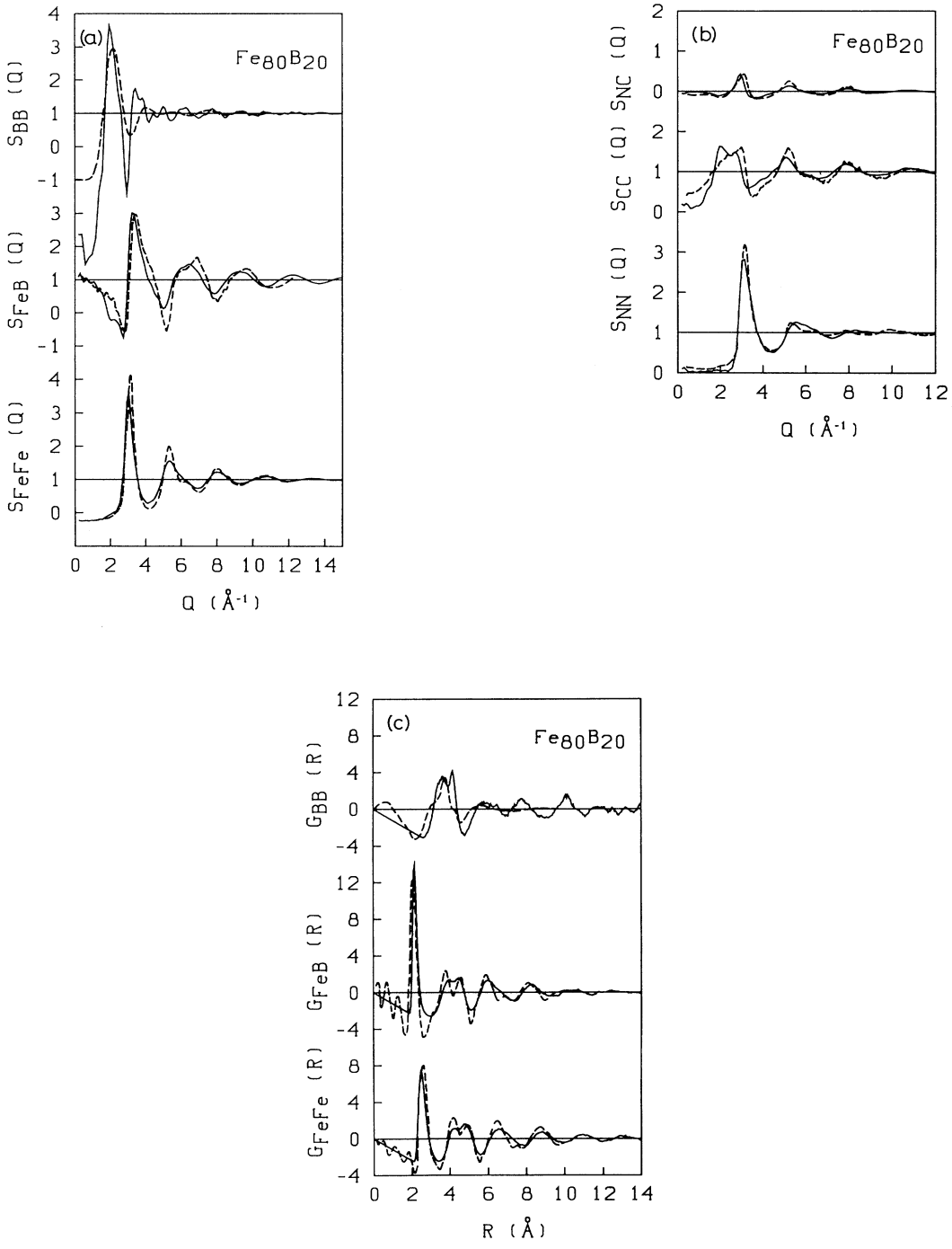

FIG. 6. (a) Faber-Ziman and (b) Bhatia-Thornton static structure factors $S_{\alpha\beta}(Q)$ and reduced radial distribution functions $G_{\alpha\beta}(R)$ for amorphous $Fe_{80}B_{20}$. Solid line, molecular-dynamics simulation, dashed line, neutron-diffraction data after Nold *et al.* (Ref. 4).

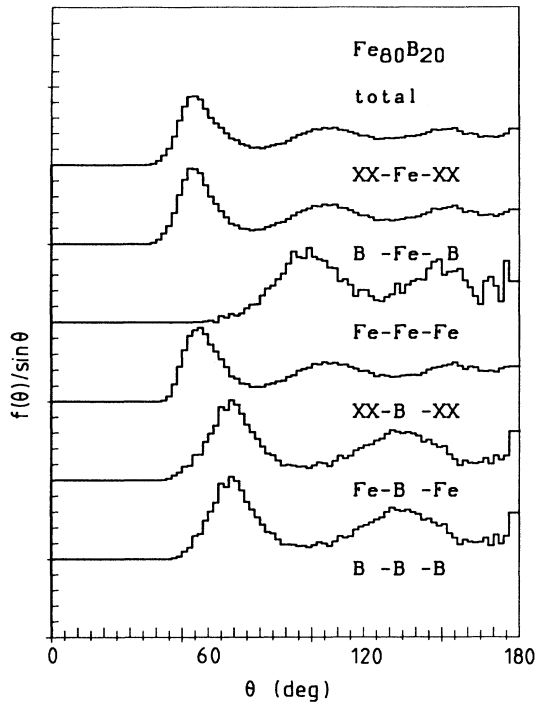

FIG. 7. Total and partial bond-angle distribution $F(\Theta)$ (normalized by $\sin^{-1}\Theta$) for $Fe_{80}B_{20}$. X=Fe or B. All distributions are normalized to the same numbers of bonds.

angles is normalized by a factor $\sin^{-1}(\Theta)$, so that a random distribution corresponds to a constant]. Around the B sites, bond angles of 72°, 130°, and 180° are most frequent. In a broad sense, this is again compatible with a trigonal-prismatic local order. The B-Fe-B bond angle carries the information on the connectivity of the local structural units.

2. $Ni_{81}B_{19}$

The results for the glass $Ni_{81}B_{19}$ are shown in Fig. 8. In this case the agreement between theory and experiment is almost perfect, see also the interatomic distances and coordination numbers given in Table II. The only difference is in the shape of the first peak of $S_{CC}(Q)$. We assume that this reflects the tendency of the theoretical model to underestimate the splitting of the first peak in $G_{BB}(R)$. The structures of a-$Fe_{80}B_{20}$ and a-$Ni_{81}B_{19}$ are found to be very similar, even more so in the theoretical model than in the data derived from the diffraction experiments. The distribution of the bond angles, however, points to certain differences in the connectivity of the trigonal prismatic units (Fig. 9). The peak in the B-Fe-B bond-angle distribution for $Fe_{80}B_{20}$ close to 145° is flattened in $Ni_{81}B_{19}$. This could be connected with the fact that while Ni_3B assumes on a Fe_3C- (cementite) type lattice, Fe_3B has the Fe_3P structure (an Fe_3C-type phase can be produced only in metastable from by liquid quenching).[75] We shall come back to this point below.

The concentration-fluctuation structure factor $S_{CC}(Q)$ shows the onset of small-angle scattering, indicating the onset of medium-range ordering [Fig. 8(b)]. This agrees with the results of Lamparter and Steeb[77] who deduced from small-angle scattering with isotopic substitution that concentration fluctuations with a correlation length of about 15 Å exist in $Ni_{80}B_{20}$. Thus, our standard models with linear dimensions of ~25 Å are just large enough to show the onset of such effects. The concentration fluctuations were assumed to arise from the formation of B-enriched regions. We shall come back to the medium-range order below.

3. $Ni_{64}B_{36}$

Amorphous $Ni_{64}B_{36}$ has been investigated by Cowlam *et al.*[8,9] as an example of a TM-M glass with direct metalloid neighbors. The calculated pair interactions are shown in Fig. 10. Compared to the Ni-rich glass, the strength of all covalent bonds is reduced, but there is no fundamental change in the interatomic forces with composition (see the pair potentials shown in Figs. 3 and 10). The experimental results are not documented in as much detail as for the Ni-rich glass, but the calculated Ashcroft-Langreth structure factors are in good agreement with experiment (Fig. 11). Compared to the Ni-rich glass, the total B coordination number is unchanged but on average one Ni neighbor is replaced by a B atom (Table II). The total Ni coordination number is increased. The interatomic distance in the direct B-B pair is d_{BB}=2.53 Å [see Fig. 11(c)], i.e., it is still slightly larger than the shortest Ni-B distance. The nearest-neighbor B-B peak overlaps with the split next-nearest-neighbor peak whose shape and position is similar as in the Ni_8B_{19} glass [compare Figs. 11(c) and 8(c)]. Gardner, Cowlam, and Davies[8] claim a shortest B-B distance of 1.8 Å. However, the amplitude of the peak assigned to B-B pairs is hardly larger that of the unphysical termination wiggles at even shorter distances, and the radial distribution function goes even negative at R ~2.2 Å. Therefore, we consider this assignment as rather uncertain. The bond-angle distribution functions suggest a substantial change of the angles formed by B-Ni-B triplets and by bonds around a central B atom (cf. Figs. 9 and 12).

It is important to note that $Ni_{64}B_{36}$ glasses show no sign of small-angle scattering in the partial structure factors. This would suggest that the medium-range concentration fluctuations detected in $Ni_{81}B_{19}$ are absent in the B-richer glass.

C. Phosphorus glasses

1. $Fe_{80}P_{20}$ and $Fe_{76}P_{24}$

The partial structure factors and correlation functions of amorphous $Fe_{76}P_{24}$ glasses have been determined by Waseda[5,78] using the anomalous x-ray-scattering technique. This method produces substantially lower resolu-

tion than the neutron-scattering techniques. This affects mainly the R-space correlation effects which are affected by truncation errors. The partial pair correlation functions for amorphous $Fe_{76}P_{24}$ and $Fe_{80}P_{20}$ are shown in Fig. 13. The computer-generated model agrees moderately well with experiment. The most serious discrepancy is in the structure of the second peak of $g_{FeP}(R)$ and $g_{FeFe}(R)$. For the Fe-P glasses we show for comparison the simulation results of Fujiwara, generated with modified Morse-type potentials. The parameters (exponent, diameter, strength, cutoff) of these potentials have been adjusted such as to produce optimum agreement with the experimental data. The results are in a surprisingly good agreement with the present work

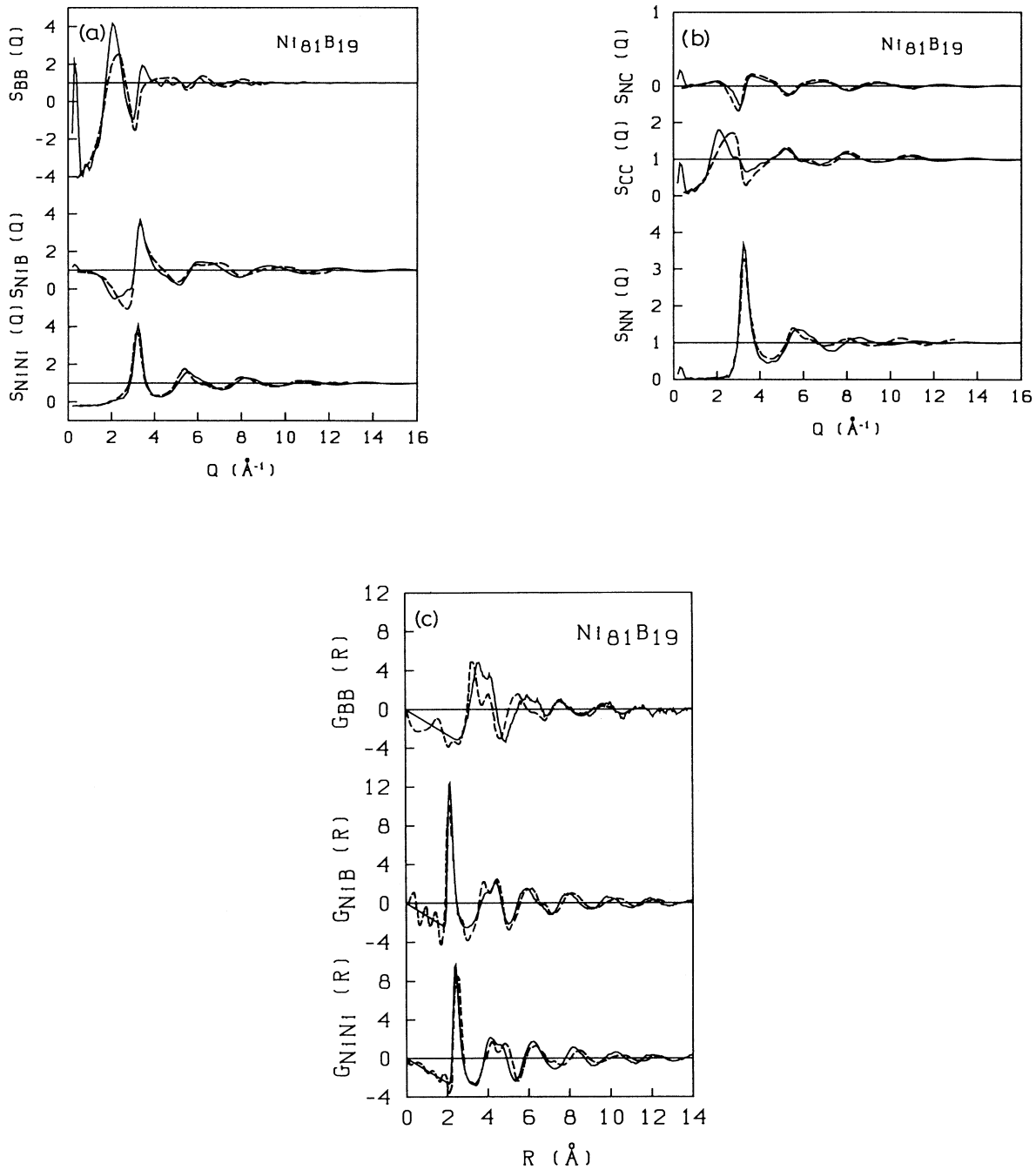

FIG. 8. (a) Faber-Ziman and (b) Bhatia-Thornton static structure factors $S_{\alpha\beta}(Q)$ and reduced radial distribution functions $G_{\alpha\beta}(R)$ for amorphous $Ni_{81}B_{19}$. Solid line, molecular-dynamics simulation; dashed line, neutron-diffraction data after Lamparter *et al.* (Ref. 7).

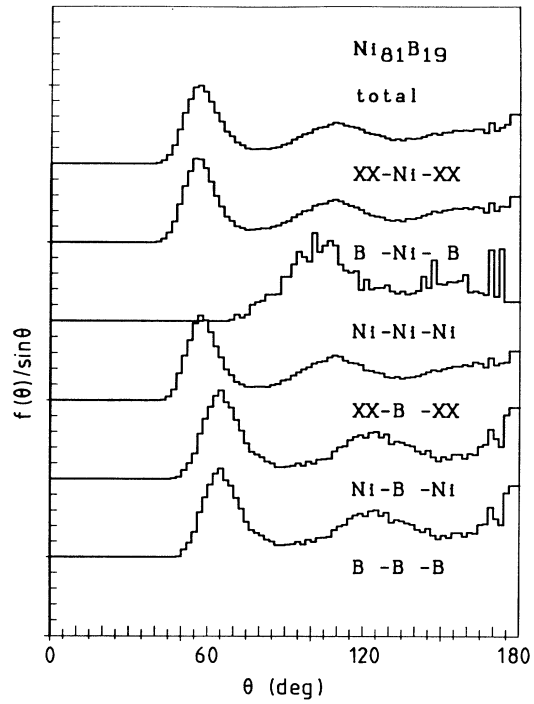

FIG. 9. Total and partial bond-angle distribution $f(\Theta)$ for $Ni_{81}B_{19}$, cf. Fig. 7.

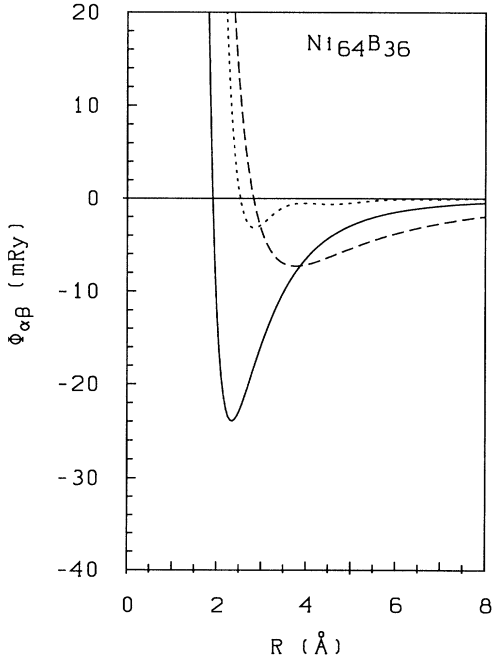

FIG. 10. Pair interactions $\Phi_{\alpha\beta}(R)$ for $Ni_{64}B_{36}$. For the key see Fig. 2.

(where there are no adjustable parameters in the quantum-mechanical pair forces). This would seem to indicate that this is about as far as one can go with central pair forces—improvements beyond that level would be possible only with angular-dependent noncentral forces. The partial structure factors (Fig. 13) indicate again a strong chemical order (see also the coordination numbers given in Table II) and a certain small-angle scattering.

2. $Ni_{80}P_{20}$

Figure 14 compares the structural models for amorphous $Ni_{80}P_{20}$ with the neutron-diffraction data of Lamparter and Steeb.[6] The agreement between theory and experiment is distinctly better than for the Fe-P glasses. This is important, since the quality of the experimental partial structure functions is superior for the Ni-based glasses. Still, in the R-space correlations we note a certain difference in the width of the first peak of the P-P correlations, and in the shape of the second peak in the Ni-P correlations. In Q space we find generally good agreement between theory and experiment, both in the Faber-Ziman and Bhatia-Thornton formalisms.

In the coordination numbers we note a certain change in the P-based glasses relative to the B glasses: at the same composition, the TM-TM coordination numbers are slightly larger in the P than in the corresponding B glasses (Table II). The change is also reflected in the distribution of the M-TM-M bond angles which is distinctly different in $Ni_{80}P_{20}$ (Fig. 15) and in the B glasses. In $Fe_{80}P_{20}$ it has an intermediate character.

For the $Ni_{80}P_{20}$ glass our simulations predict the most intense small-angle scattering in the $S_{PP}(Q)$ and $S_{CC}(Q)$ structure factors. If these long-wavelength concentration fluctuations are indeed caused by the formation of metalloid-rich regions, then our predictions for $Fe_{80}P_{20}$ and $Ni_{80}P_{20}$ correlate with the Guinier analysis of the small-angle scattering[77,79] suggesting a large volume fraction of enriched regions in amorphous $Ni_{80}P_{20}$ (Ref. 80) and a strong decrease with substitution of Ni by Fe at a constant TM-M ratio.[81]

D. Short-range order

The coordination numbers and interatomic distances compiled in Table II indicate that the topology of the local atomic environment is, in general, well described by our simulation. In particular, we stress that TM-TM and M-TM distances are predicted with a maximum error of 0.1 Å. This is certainly a rather stringent test of the accuracy of the tight-binding-bond forces. The coordination numbers are also predicted with good accuracy, although one should remember that there is considerable uncertainty due to the various possible ways to define a coordination number (for a discussion see, e.g., Waseda[78]). These results are certainly compatible with a trigonal prismatic coordination of the metalloid atoms by metal atoms.

Various attempts have been made to extract informa-

tion on the way these prismatic units are packed together. This is the point where the models generated by sphere-packing, molecular-dynamics, or Monte Carlo algorithms are essentially different from stereochemically defined models.[21] In the former, trigonal-prismatic local order may appear as a consequence of a particular interatomic potential, but the connectivity of the local units is expected to be random. In the stereochemically defined models, edge sharing is imposed as an additional constraint. Gaskell[21] has tried to relate the interatomic distances characterizing the different possible edge-sharing arrangements of prisms characteristic for the crystalline Fe_3C and Fe_3P phases to particular features of the partial correlation functions. An Fe_3C-type packing leads to a

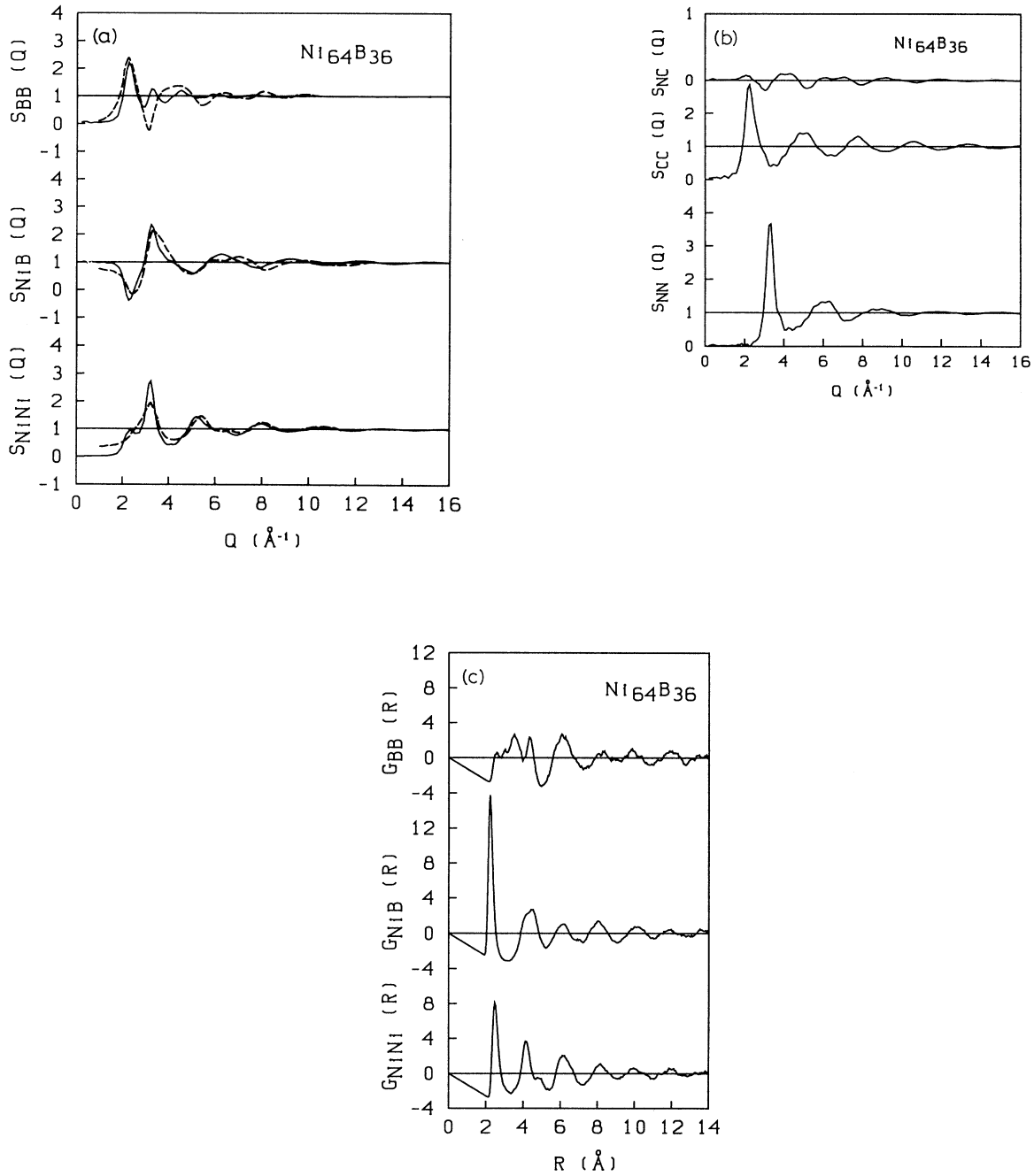

FIG. 11. (a) Ashcroft-Langreth and (b) Bhatia-Thornton partial structure factors $S_{\alpha\beta}(Q)$ and reduced distribution functions $G_{\alpha\beta}(R)$ (c) for amorphous $Ni_{64}B_{36}$. Solid line, molecular-dynamics simulation; dashed line, neutron-diffraction data of Gardner *et al.* (Refs. 8, 9, and 76).

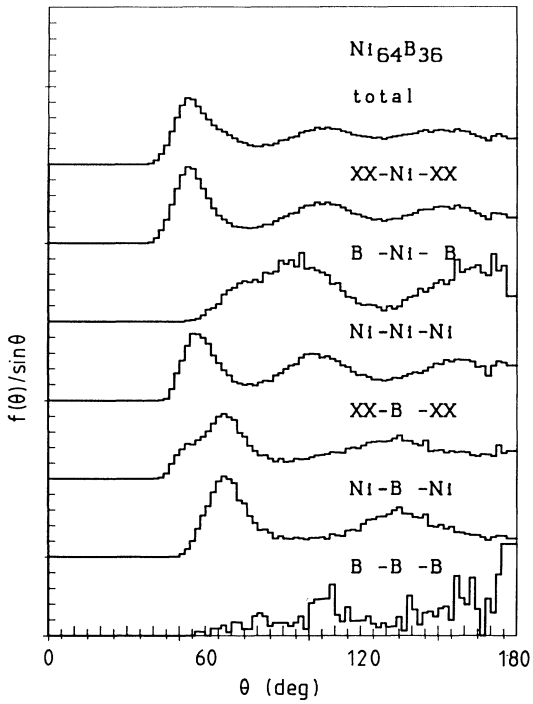

FIG. 12. Total and partial bond-angle distributions $f(\Theta)$ for $Ni_{64}B_{36}$, cf. Fig. 7.

second-neighbor M-TM distance across a tetrahedral and an octahedral hole (T-O), and an Fe_3 P-type packing to a tetrahedral-tetrahedral (T-T) packing. This leads to two characteristic distances that may be compared to the TM-M correlation function (see Ref. 21, p. 42, for details). This is done in Fig. 16. We find that for $Ni_{81}B_{19}$ the shoulder on the left side of the second peak agrees somewhat better with the T-O distance (and hence Fe_3C-type packing), whereas for $Fe_{80}B_{20}$ the correlation is better with the T-T distance (and hence Fe_3P-type packing). This would agree with the stable crystal structures of the Ni_3B and Fe_3B phases. For the P glasses there is no clear distinction. Gaskell's random trigonal-prismatic models with imposed cementite-type edge sharing show a split second peak, indicating that the arrangement of the tetrahedra is defined more sharply than in our model. A more pronounced structure would also improve the detailed agreement of our model with experiment, but, on the other hand, our model predicts second-neighbor distances better than Gaskell's model.

From this we conclude that our quantum-mechanical central-force model describes the bonding in TM-M glasses very well, including the formation of trigonal-prismatic units. However, angular-dependent forces will eventually be necessary to produce more sharply defined correlations between these local units.

E. Medium-range order

While it seems that the short-range order in TM-M glasses is reasonably well described in terms of a packing of slightly distorted trigonal-prismatic units and that the stability and connectivity of these units is due to strong nonadditive covalent bonding forces, much less is known about the medium-range order. From the analysis of neutron- and x-ray small-angle scattering data[77,80–82] and from field ion microscopy,[83] it was concluded that medium-range order in TM-M glasses involves two characteristic length scales: (i) Concentration fluctuations with a correlation length of typically 15 Å in quenched samples, associated with the formation of B-enriched regions in T_xB_{1-x} glasses with $x \geq 0.8$. Within the B-enriched regions the stoichiometry of the glass should be close T_3B, corresponding to the stable Fe_3C- and Ni_3P-type phases. No concentration fluctuations are detected for $x \leq 0.75$. The incipient phase separation is enhanced by neutron irradiation causing the formation of excess free volume. (ii) Density fluctuations on a length scale of several hundred Å (corresponding to $Q < 0.1$ $Å^{-1}$).

It is impossible to perform computer simulations at these large scales, and even for the fluctuations at small scale, the correlation length is dangerously close to the linear dimensions of a typical MD sample. Therefore, it is not meaningful to attempt a detailed analysis of the small-angle scattering (SAS) that shows up in the concentration-fluctuation structure factors $S_{CC}(Q)$ of $Ni_{81}B_{19}$ (but not $Ni_{64}B_{36}$), $Fe_{80}B_{20}$, $Ni_{80}P_{20}$, and to a lesser extent, in $Fe_{80}P_{20}$. The onset of the SAS occurs typically at $Q \leq 0.5$–0.6 $Å^{-1}$, in agreement with experimental observation. For a 1500-atom model and periodic boundary conditions, the scattering intensity can be calculated only for $Q \geq 0.25$ $Å^{-1}$ at the densities of the TM-M glasses. However, unlike a laboratory experiment, a computer experiment allows one to visualize the $3d$ atomic scale structure of the sample.

Figure 17 shows a projection of a slice of a 1372-atom model onto the (x,y) plane. The thickness of the slice is 7 Å, i.e., slightly larger than two TM-M bond lengths. TM and M atoms are drawn together with the network of M-TM nearest-neighbor bonds. The size of the symbols is scaled with the z coordinate, atoms close to the upper surface appearing larger. The overall density of Ni atoms appears to be quite homogeneous, but if the Ni atoms are omitted for the sake of clearity, we see that there are fluctuations in the local distribution of the B atoms. No such fluctuations are found in $Ni_{64}B_{36}$ [Figs. 17(c) and 17(d)]. Strong concentration fluctuations are observed in $Ni_{80}P_{20}$: a small region is completely depleted of P atoms [Figs. 17(e) and 17(f)]. A similar, though less pronounced, effect is also found in $Fe_{80}P_{20}$ [Figs. 17(g) and 17(h)]. The correlation length of thee concentration fluctuations appears to be compatible with the experimental estimate. It is also characteristic that concentration fluctuations are not observed in smaller molecular-dynamics (MD) samples ($N \leq 500$ atoms). We also find that a lower density enhances the trend to phase separation.

Of course, we have to admit that these results depend to some degree on the parametrization of the repulsive forces between the metalloid atoms (cf. Sec. III C). Here it is important to emphasize that we use the *same* parameter in the repulsive B-B interactions in all boride glasses

and at all compositions (no adjustment was made for the phosphide glasses). Hence, the concentration dependence of the medium-range order shown in Fig. 17 should not be the result of our choice of parameters. At the moment, an improved TB parametrization of B must be left to future studies. This will be a rather difficult task, since the existing database for such a parametrization is much narrower than, e.g., for C.

Hence we conclude that the medium-range concentration fluctuations arise from the strong M-TM bonding. For packing reasons, a B atom can be surrounded by at most 9–10, a P atom by up to 11 neighbors. Due to the

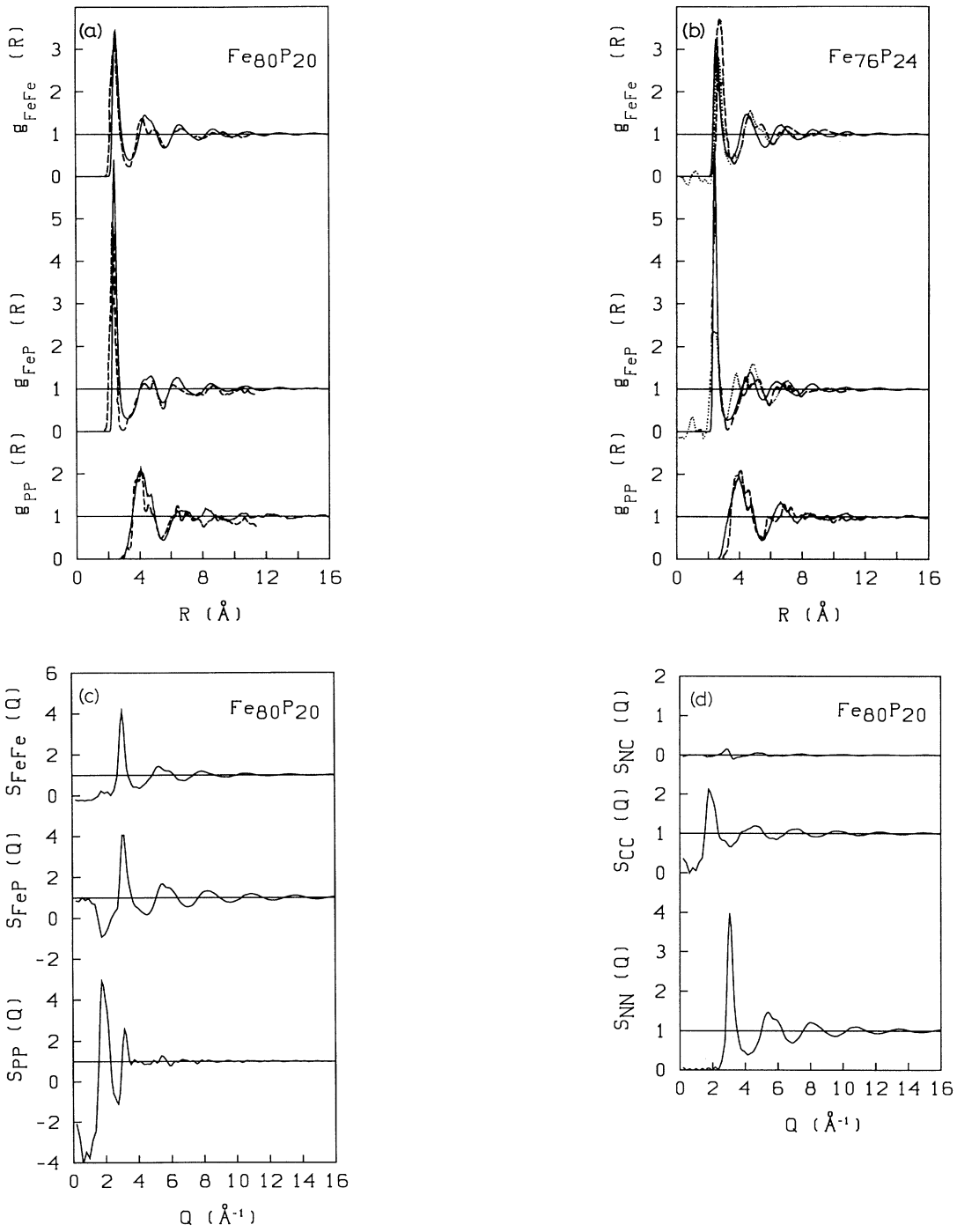

FIG. 13. Partial pair correlation functions $g_{\alpha\beta}(R)$ for amorphous (a) and (b) $Fe_{80}P_{20}$ and $Fe_{76}P_{24}$ and (c) Faber-Ziman and (d) Bhatia-Thornton partial structure factors for a-$Fe_{80}P_{20}$. Solid line, present MD simulations; dashed line, static relaxation calculations of Fujiwara [with prescribed chemical short-range order in the starting model (Ref. 5)]; dotted curve, experimental results of Waseda *et al.* (Refs. 5 and 78).

strong attractive M-TM forces it is energetically favorable to saturate the maximum allowable number of bonds. Our present MD simulation leads to a qualitatively correct description of medium-range ordering. However, much larger models are required for more than a semiquantitative interpretation of the SAS data.

V. DISCUSSION

We have shown that a simple TM-*d*-M-*p* bond model can account quantitatively for the interatomic forces in disordered transition-metal–metalloid alloys. The strong covalent character of the bond is reflected in the pronounced nonadditivity of the interatomic pair forces.

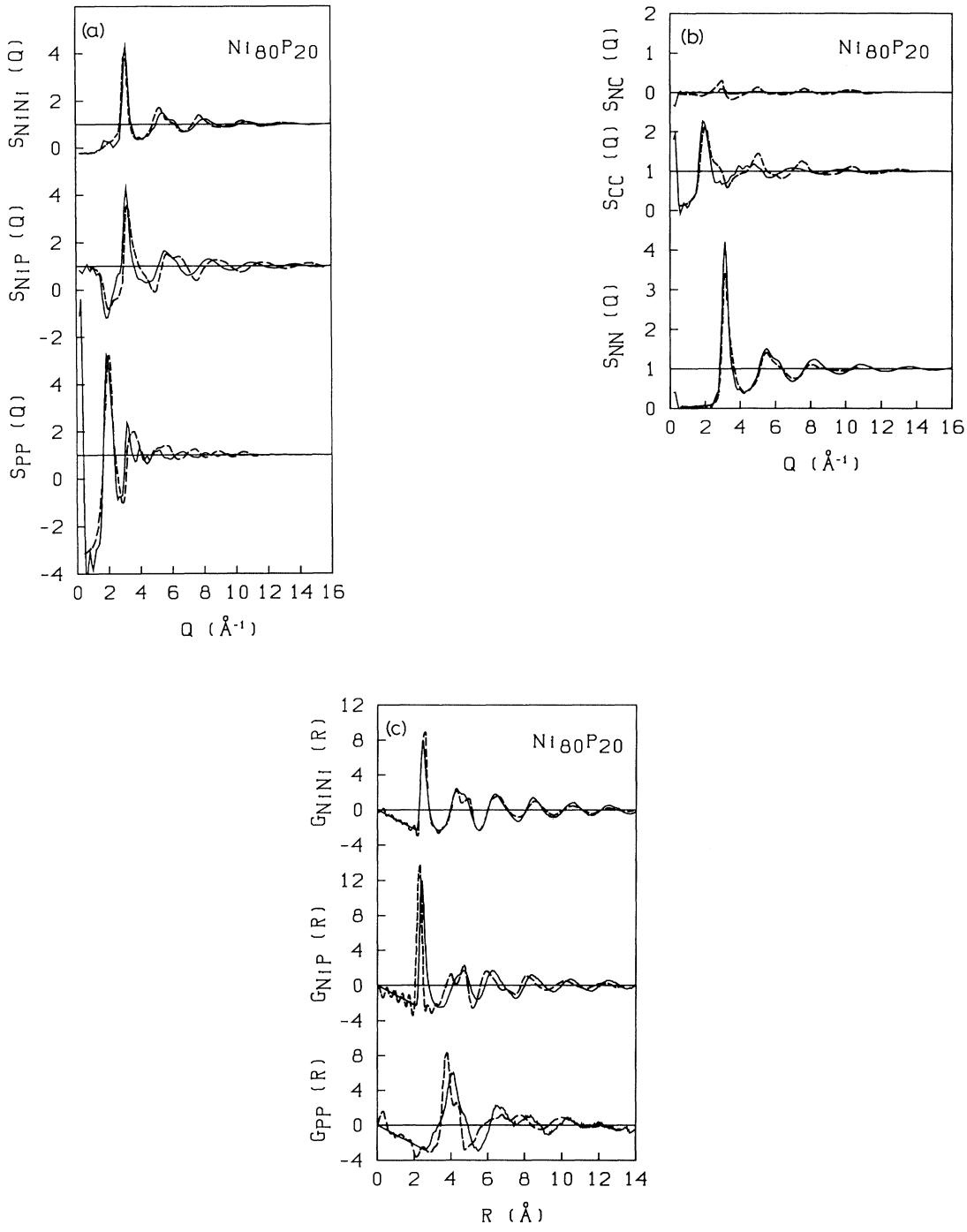

FIG. 14. (a) Faber-Ziman and (b) Bhatia-Thornton static structure factors $S_{\alpha\beta}(Q)$ and reduced radial distribution functions $G_{\alpha\beta}(R)$ for amorphous $Ni_{80}P_{20}$. Solid lines, molecular-dynamics simulation; dashed lines, neutron-diffraction results of Lamparter and Steeb (Ref. 6).

This nonadditivity is sufficient to reproduce the main features of the short-range order in the glassy phase: strong chemical ordering and at least a certain tendency to a trigonal-prismatic topological short-range order related to the structure of the stable crystalline phases. There are certain indications in the measured correlation functions that the local topology is somewhat more sharply defined in the real material than in our models. To eliminate these remaining small differences it will be necessary to go beyond the pair-potential approximation. However, both the quantum-mechanical calculation of angular-dependent forces by a moment expansion of the bond order and their use in MD simulations constitute a considerable complication.

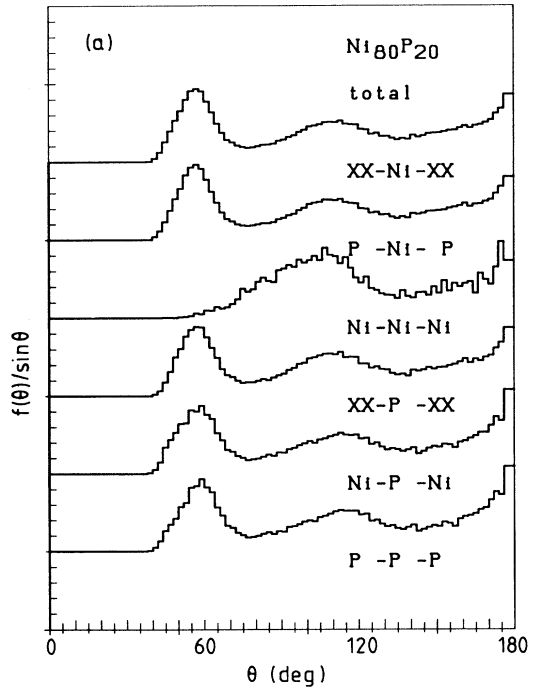

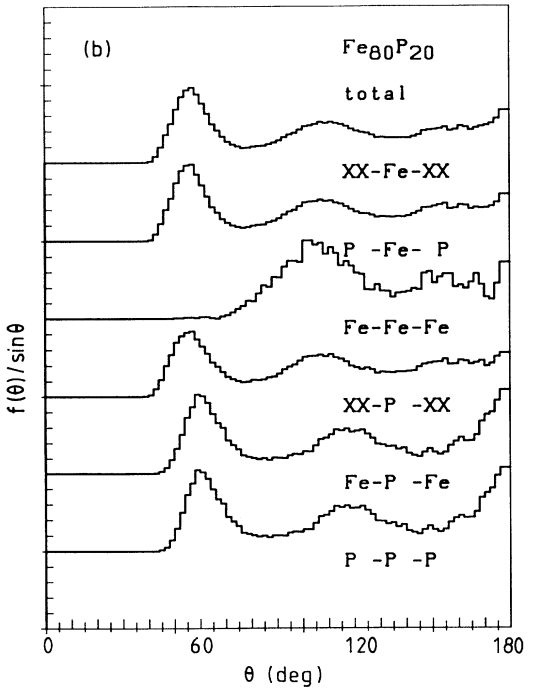

FIG. 15. Bond-angle distributions in amorphous (a) $Ni_{80}P_{20}$ and (b) $Fe_{80}P_{20}$, cf. Fig. 7.

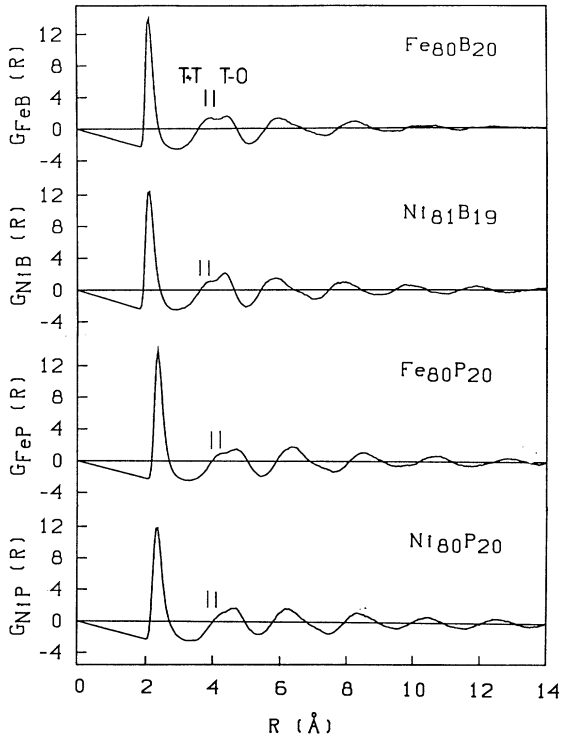

FIG. 16. TM-M pair correlation functions for (Fe,Ni)-(B,P) glasses. The vertical bars labeled T-T and T-O indicate the tetrahedron-tetrahedron and tetrahedron-octahedron packing of trigonal prisms characteristic for a Fe_3P- and Fe_3C-type connectivity of the trigonal prisms.

Our simulations also indicate the existence of concentration fluctuations on a length scale of 15–20 Å, in agreement with small-angle scattering data. The semiquantitative prediction of these medium-range fluctuations and of their concentration dependence is certainty remarkable. However, a quantitative analysis of the existing SAS data will require simulation on much larger ensembles. Such calculations for systems with several 10^4 atoms are now under way and preliminary results look promising. The new structural models also allow for an investigation of the electronic and magnetic properties of TM-M glasses and a discussion of the interplay between the atomic and electronic properties on a microscopic basis.

Note added in proof. The molecular-dynamics simulations of the structure of Fe_xB_{1-x} glasses ($x=0.9$, 0.80, 0.85, and 0.75) have been repeated from models containing 10^4 atoms in the periodic cell.[84] The results confirm the conclusions drawn on the basis of the smaller ensem-

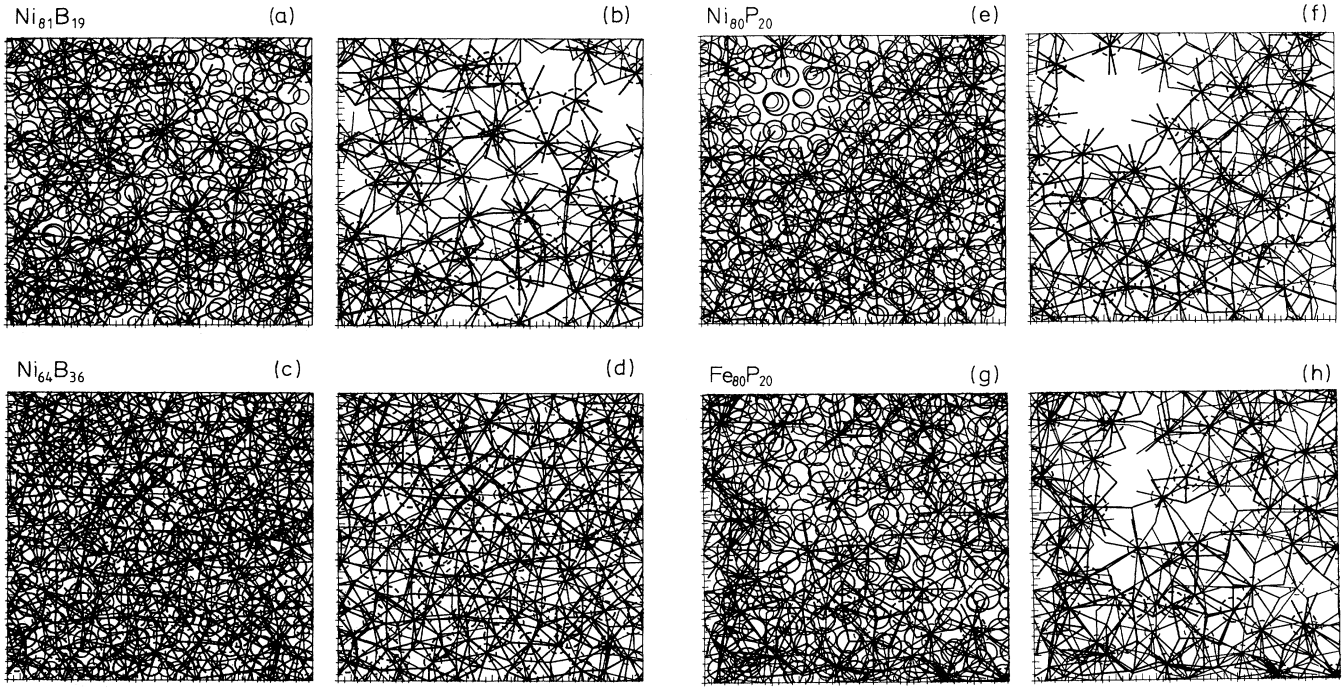

FIG. 17. Projection of part of an $N=1372$-atom model of the amorphous structure on the (x,y) plane. Solid circles, TM atoms; dashed circles, M atoms. Solid lines show nearest-neighbor M-TM bonds. Left part; projection of all atoms; right part; TM atoms are omitted for sake of clarity. See text. (a) and (b) $Ni_{81}B_{19}$, (c) and (d) $Ni_{64}B_{36}$, (e) and (f) $Ni_{80}P_{20}$, and (g) and (h) $Fe_{80}P_{20}$.

bles and show that a quantitative interpretation of the SAS data is possible. The structural models discussed in this paper have been used as the basis of spin-polarized electronic structure calculations[85] for Fe_xB_{1-x} glasses. The results show that Fe-rich Fe-B glasses are weak ferrimagnets (positive moments on the Fe sites, small negative moments on the B sites). The calculated variation of the magnetic moment with composition is in full agreement with experiment.

ACKNOWLEDGMENT

This work has been supported by the Hochschuljuliläums-Stiftung der Stadt Wien.

APPENDIX

Expressions for the coefficients A_i in the quartic equation (2.15) are given below.

$$A_4=\frac{Z_\beta-1}{Z_\beta}\frac{Z_{\alpha\alpha}^2 Z_{\beta\beta}}{Z_{\alpha\beta}^2}\frac{t_{\alpha\alpha}^2 t_{\beta\beta}^2}{t_{\alpha\beta}^4}-\frac{Z_\beta-1}{Z_\beta}\frac{Z_{\alpha\alpha}Z_{\beta\alpha}}{Z_{\alpha\beta}},$$

$$A_3=\frac{Z_\alpha}{Z_\beta}\frac{Z_\beta-1}{Z_\alpha-1}\left[\frac{Z_{\beta\alpha}}{Z_{\alpha\beta}}-2\frac{Z_{\alpha\alpha}Z_{\beta\beta}}{Z_{\alpha\beta}^2}\cdot\frac{t_{\alpha\alpha}^2 t_{\beta\beta}^2}{t_{\alpha\beta}^4}\right]\frac{E-E^\alpha}{t_{\alpha\alpha}}+\frac{Z_{\alpha\alpha}}{Z_{\alpha\beta}}\frac{t_{\alpha\alpha}t_{\beta\beta}}{t_{\alpha\beta}^2}\frac{E-E^\beta}{t_{\beta\beta}},$$

$$A_2=\frac{Z_\alpha^2}{(Z_\alpha-1)^2}\frac{Z_\beta-1}{Z_\beta}\frac{Z_{\beta\beta}}{Z_{\alpha\beta}^2}\frac{t_{\alpha\alpha}^2 t_{\beta\beta}^2}{t_{\alpha\beta}^4}\frac{(E-E^\alpha)^2}{t_{\alpha\alpha}^2}+2\frac{Z_\alpha}{Z_\beta}\frac{Z_\beta-1}{Z_\alpha-1}\frac{Z_{\alpha\alpha}Z_{\beta\beta}}{Z_{\alpha\beta}^2}\frac{t_{\alpha\alpha}^2 t_{\beta\beta}^2}{t_{\alpha\beta}^4}$$

$$-\frac{Z_\alpha}{Z_\alpha-1}\frac{1}{Z_{\alpha\beta}}\frac{(E-E^\alpha)(E-E^\beta)}{t_{\alpha\alpha}t_{\beta\beta}}\frac{t_{\alpha\alpha}t_{\beta\beta}}{t_{\alpha\beta}^2}-\frac{Z_\alpha}{Z_\beta}\frac{Z_\beta-1}{Z_\alpha-1}\frac{Z_{\beta\alpha}}{Z_{\alpha\beta}}+1,$$

$$A_1=\frac{Z_\alpha}{Z_\alpha-1}\left[\frac{1}{Z_{\alpha\beta}}\frac{t_{\alpha\alpha}t_{\beta\beta}}{t_{\alpha\beta}^2}\frac{(E-E^\beta)}{t_{\beta\beta}}-2\frac{Z_\alpha}{Z_\beta}\frac{Z_\beta-1}{Z_\alpha-1}\frac{Z_{\beta\beta}}{Z_{\alpha\beta}^2}\frac{t_{\alpha\alpha}^2 t_{\beta\beta}^2}{t_{\alpha\beta}^4}\frac{E-E^\alpha}{t_{\alpha\alpha}}\right],$$

$$A_0=\frac{Z_\alpha^2}{(Z_\alpha-1)^2}\frac{Z_\beta-1}{Z_\beta}\frac{Z_{\beta\beta}}{Z_{\alpha\beta}^2}\frac{t_{\alpha\alpha}^2 t_{\beta\beta}^2}{t_{\alpha\beta}^4},\quad \alpha,\beta=A,B\ \alpha\neq\beta.$$

[1]A. Brenner, D. E. Couch, and E. K. Williams, J. Res. Natl. Bur. Stand. **44**, 109 (1950).
[2]P. Duwez, R. H. Wilens, and W. Klement, J. Appl. Phys. **31**, 120 (1960).
[3]K. Moorjani and J. M. D. Coey, *Magnetic Glasses* (Elsevier, Amsterdam, 1984), Chap. VIII.
[4]E. Nold, P. Lamparter, H. Olbrich, G. Rainer-Harbach, and S. Steeb, Z. Naturforsch. Teil A **36**, 1032 (1981).
[5]T. Fujiwara, H. S. Chen, and Y. Waseda, Z. Naturforsch. Teil A **37**, 611 (1982); J. Phys. F. **11**, 1327 (1981).
[6]P. Lamparter and S. Steeb, in *Rapidly Quenched Metals V,* edited by S. Steeb and H. Warlimont (Elsevier, Amsterdam, 1985), p. 459.
[7]P. Lamparter, W. Sperl, and S. Steeb, Z. Naturforsch. Teil A **37**, 1223 (1982).
[8]P. P. Gardner, N. Cowlam, and H. A. Davies, J. Phys. F **15**, 769 (1985).
[9]P. Gardner and N. Cowlam, J. Phys. F **15**, 2553 (1985).
[10]P. Kizler, P. Lamparter, and S. Steeb, Z. Naturforsch. Teil A **43**, 1047 (1988).
[11]M. Matsumura, T. Nomoto, F. Itoh, and K. Suzuki, Solid State Commun. **33**, 895 (1980).
[12]A. Amamou and G. Krill, Solid State Commun. **33**, 1029 (1980).
[13]T. Honda, F. Itoh, and K. Suzuki, in *Rapidly Quenched Metals IV,* edited by T. Masumoto and K. Suzuki (The Japan Institute of Metals, Sendai, 1981), p. 1303.
[14]E. Colavita, M. de Crescenzi, L. Papagno, R. Scarremozino, G. Chiarello, L. S. Caputi, and R. Rosei, in *Rapidly Quenched Metals IV,* edited by T. Masumoto and K. Suzuki (The Japan Insitute of Metals, Sendai, 1981), p. 1271.
[15]K. Tanaka, M. Yashino, and K. Suzuki, results reported in *Amorphous Materials: Modeling of Structure and Properties,* (Ref. 16).
[16]T. Fujiwara, in *Amorphous Materials: Modeling of Structure and Properties,* edited by V. Vitek (The Metallurgical Society of AIME, Warrendale, 1983), p. 221.
[17]K. Moorjani and J. M. D. Coey, *Magnetic Glasses* (Ref. 3), p. 92ff.
[18]K. Fukamichi, M. Kikuchi, H. Hiroyoshi, and T. Masumoto, in *Rapidly Quenched Metals III,* edited by B. Cantor (The Metals Society, London, 1978), Vol. 2, p. 325.
[19]F. E. Luborsky, H. H. Liebermann, J. J. Becker, and J. L. Walter, in *Rapidly Quenched Metals III* (Ref. 18), Vol. 2, p. 188.
[20]N. Cowlam and G. E. Carr, J. Phys. F **15**, 1109 (1985); **15**, 1117 (1985).
[21]P. H. Gaskell, in *Glassy Metals II,* edited by H. Beck and H. J. Güntherodt (Springer, Berlin, 1983), p. 5.
[22]For a recent review, see, e.g., R. E. Watson and L. H. Bennett, Phys. Rev. B **43**, 11 642 (1991).
[23]T. Fujiwara and Y. Ishii, J. Phys. F **10**, 1091 (1980).
[24]L. J. Lewis and R. Harris, J. Non-Cryst. Solids **61+62**, 547 (1984).
[25]T. A. Weber and F. H. Stillinger, Phys. Rev. B **31**, 1954 (1985).
[26]O. Beyer and C. Hoheisel, Z. Naturforsch. Teil A **38**, 859 (1983).
[27]E. H. Brandt and H. Kronmüller, J. Phys. F **17**, 1291 (1987).
[28]A. M. Bratkovsky and A. V. Smirnov, J. Phys. Condens. Matter **3**, 5153 (1991).
[29]A. P. Malozemoff, A. R. Williams, and V. L. Moruzzi, Phys. Rev. B **29**, 1620 (1984).
[30]M. Krajči and P. Mrafko, J. Phys. F **18**, 2137 (1988).
[31]T. Fujiwara, J. Phys. F **12**, 661 (1982).
[32]W. Y. Ching, J. Non-Cryst. Solids **75**, 379 (1985).
[33]W. Y. Ching, L. W. Song, and S. S. Jaswal, Phys. Rev. B **30**, 544 (1984).
[34]X. F. Zhong, Y. N. Xu, and W. Y. Ching, Phys. Rev. B **41**, 10 545 (1991).
[35]S. Krompieswski, U. Krey, and H. Ostermeier, J. Magn. Magn. Mater. **69**, 117 (1987); **73**, 5 (1988).
[36]C. A. Coulson, Proc. R. Soc. London Ser. A **169**, 413 (1939).
[37]G. C. Abell, Phys. Rev. B **31**, 6184 (1984).
[38]A. P. Sutton, M. W. Finnis, D. G. Pettifor, and Y. Ohta, J. Phys. C **21**, 35 (1988).
[39]D. G. Pettifor, Phys. Rev. Lett. **63**, 2480 (1989).
[40]D. G. Pettifor and M. Aoki, Philos. Trans. R. Soc. London, Ser. A **334**, 439 (1991).
[41]Ch. Hausleitner and J. Hafner, Phys. Rev. B **45**, 115 (1992).
[42]W. Jank, Ch. Hausleitner, and J. Hafner, Europhys. Lett. **16**, 473 (1991); Ch. Hausleitner, M. Tegze, and J. Hafner, J. Phys. Condens. Matter **4**, 9557 (1992).
[43]P. Oelhafen, in *Glassy Metals II* (Ref. 21), p. 283.
[44]Ch. Hausleitner and J. Hafner, Phys. Rev. B **45**, 128 (1992).
[45]Ch. Hausleitner and J. Hafner, J. Non-Cryst. Solids **144**, 175 (1992).
[46]D. J. Joyner, O. Johnson, D. B. Hercules, D. W. Bullett, and J. D. Weaver, Phys. Rev. B **24**, 3122 (1981).
[47]P. Mohn and D. G. Pettifor, J. Phys. C **21**, 2829 (1988); P. Mohn, *ibid.* **21**, 2841 (1988).
[48]W. Y. Ching, Y. N. Xu, B. N. Harmon, J. Ye, and T. C. Leung, Phys. Rev. B **42**, 4460 (1990).
[49]D. G. Pettifor and R. Podloucky, J. Phys. C **19**, 315 (1986).
[50]E. N. Economou, *Greens Functions in Quantum Physics* (Springer, Berlin, 1979), p. 232.
[51]D. Nguyen Manh, G. Dinh Hoai, A. Pasturel, and C. Colinet, Physica B **173**, 293 (1991).
[52]A. Z. Maksymovicz, Phys. Status. Solid B **122**, 519 (1984); K. Swiderczak, A. Zagorski, and J. Krol, *ibid.* **134**, 581 (1986).
[53]V. Heine and D. Weaire, *Solid State Physics,* edited by H. Ehrenreich, D. Turnbull, and F. Seitz (Academic, New York, 1970), Vol. 24, p. 247.
[54]J. Hafner, *From Hamiltonians to Phase Diagrams* (Springer, Berlin, 1987).
[55]D. G. Pettifor, in *Many-Atom Interactions in Solids,* edited by R. Nieminen, M. J. Puska, and M. J. Manninen (Springer, Berlin, 1990), p. 64.
[56]V. L. Moruzzi, Ph.D. thesis Techn. University Wien, 1985 (unpublished).
[57]D. G. Pettifor, Commun. Phys. **1**, 141 (1976).
[58]D. G. Pettifor, J. Chem. Phys. **69**, 2930 (1978).
[59]O. K. Andersen and H. R. Machkintosh, in *Electrons at the Fermi Surface,* edited by M. Springford (Cambridge University Press, Cambridge, England, 1980), Sec. 5.3.
[60]L. Goodwin, A. J. Skinner, and D. G. Pettifor, Europhys. Lett. **9**, 701 (1989); L. Goodwin, J. Phys. Condens. Matter **3**, 3869 (1991).
[61]J. M. Wills and W. A. Harrison, Phys. Rev. B **28**, 4363 (1983).
[62]H. Shiba, Prog. Theor. Phys. **46**, 77 (1971).
[63]W. A. Harrison, *Electronic Structure and the Properties of Solids* (Freeman, San Francisco, 1980).
[64]O. K. Andersen and O. Jepsen, Physica B **91**, 317 (1977).
[65]W. A. Harrison and G. K. Straub, Phys. Rev. B **36**, 2695 (1987).
[66]S. Lee, Acc. Chem. Res. **24**, 249 (1991).
[67]J. C. Cressoni and D. G. Pettifor, J. Phys. Condens. Matter **3**, 495 (1991).
[68]N. W. Ashcroft, Phys. Lett. **23**, 48 (1966).

[69]Ch. Hausleitner, G. Kahl, and J. Hafner, J. Phys. Condens. Matter. **3**, 1589 (1991); W. Jank, Ch. Hausleitner, and J. Hafner, *ibid.* **3**, 4477 (1991).
[70]S. Ichimaru and K. Utsumi, Phys. Rev. B **24**, 7385 (1981).
[71]W. Y. Ching and Y. N. Xu, J. Appl. Phys. **70**, 6305 (1991)
[72]C. W. Gear, *Numerical Initial Value Problems in Ordinary Differential Equations* (Prenctice Hall, Englewood Cliffs, New Jersey, 1966), Chaps. 9 and 10.
[73]A. Arnold, N. Mauser, and J. Hafner, J. Phys. Condens. Matter **1**, 965 (1989).
[74]A. Arnold and N. Mauser, Comput. Phys. Commun. **59**, 267 (1990).
[75]P. Villars and L. D. Calvert, *Pearsons Handbook of Crystallographic Data for Intemetallic Phases* (American Society for Metals, Metals Park, 1985), Vols. 1–3.
[76]N. Cowlam, Wu Guoan, P. P. Gardner, and H. A. Davies, J. Non-Cryst. Solids **61+62**, 337 (1984).
[77]P. Lamparter and S. Steeb, J. Non-Cryst. Solids **106**, 137 (1988).
[78]Y. Waseda, *The Structure of Non-Crystalline Materials* (McGraw-Hill, New York, 1980).
[79]A. Guinier and G. Fournet, *Small Angle Scattering of X-rays* (Wiley, New York, 1955).
[80]K. Schild, F. Frisius, P. Lamparter, and S. Steeb, Z. Naturforsch. Teil A **40**, 551 (1985).
[81]R. Gerling, F. P. Schimanski, and R. Wagner, Acta Metall. **36**, 575 (1988).
[82]A. R. Yavari, in *Rapidly Quenched Metals V* (Ref. 6), p. 459.
[83]J. Piller and P. Haasen, Acta Metall. **30**, 1 (1982).
[84]Ch. Becker, J. Hafner, and Ch. Hausleitner (unpublished).
[85]M. Tegze, J. Hafner, and Ch. Hausleitner, J. Non-cryst. Solids (to be published).